

---

# MIO: MUTUAL INFORMATION OPTIMIZATION USING SELF-SUPERVISED BINARY CONTRASTIVE LEARNING

---

**Siladitya Manna**

Computer Vision and Patter Recognition Unit  
Indian Statistical Institute, Kolkata, India  
siladitya\_r@isical.ac.in

**Saumik Bhattacharya**

Department of Electronics and Electrical Communication Engineering  
Indian Institute of Technology Kharagpur, India  
saumik@ece.iitkgp.ac.in

**Umapada Pal**

Computer Vision and Patter Recognition Unit  
Indian Statistical Institute, Kolkata, India  
umapada@isical.ac.in

## ABSTRACT

Self-supervised contrastive learning is one of the domains which has progressed rapidly over the last few years. Most of the state-of-the-art self-supervised algorithms use a large number of negative samples, momentum updates, specific architectural modifications, or extensive training to learn good representations. Such arrangements make the overall training process complex and challenging to realize analytically. In this paper, we propose a mutual information optimization based loss function for contrastive learning where we model contrastive learning into a binary classification problem to predict if a pair is positive or not. This transition of the problem not only helps us to track the problem mathematically but also helps us to outperform existing algorithms. Unlike the existing methods that only maximize the mutual information in a positive pair, the proposed loss function optimizes the mutual information in both positive and negative pairs. We also present a mathematical expression for the parameter gradients flowing into the projector and the position of the feature vectors in the feature space, which helps us get a mathematical insight into the working principle of contrastive learning. We also use an additional  $L_2$  regularizer to prevent diverging of the feature vectors and improve performance. The proposed method outperforms the state-of-the-art algorithms on benchmark datasets like STL-10, CIFAR-10, CIFAR-100. After only 250 epochs of pre-training, the proposed model achieves the best accuracy of 85.44%, 60.75%, 56.81% on CIFAR-10, STL-10, CIFAR-100 datasets, respectively.

## 1 Introduction

Self-supervised learning is getting popular nowadays. The primary objective of self-supervised learning is to learn representations from data without human-annotated labels. Self-supervised learning generally consists of two phases: (1) Pre-training (or Pretext) and (2) Downstream (or target). The representations learned by the encoder in the pre-training phase are used in the downstream task in the form of transferred weights. Thus, the primary purpose of the pre-training phase is to learn weights that provide a better initialization point for the target task as the higher-level representations become more correlated to the features on the target dataset. Often, the dataset on which the model is trained is the same as the dataset that will be used in the downstream task. However, the domain of self-supervised learning is still an open research area for exploration and improvement.

## 1.1 Literature Survey

During the initial days of self-supervised learning, a lot of research was done on handcrafting pre-training tasks, also known as pretext tasks. These handcrafted tasks include geometric transformation prediction [1, 2, 3], context prediction [4, 5], jigsaw puzzle solving [6, 7, 8, 9], temporal order related tasks for videos [10, 11, 12, 13, 14], pace prediction in videos [15], image colorization [16], etc. These pretext tasks are aimed at learning representations that are invariant to transformations, context, etc. Although these tasks successfully rolled the wheels of self-supervised learning, the performance of the models pre-trained with these tasks was not at par with their supervised counterparts on the target tasks.

Several algorithms like SimCLR [17], MoCov1 [18], MoCov2 [19], BYOL [20], SimSiam [21], Barlow Twins [22] have emerged over the course of the last few years. Some of these algorithms like SimCLR [17], MoCov1 [18], MoCov2 [19], SimSiam [21] are based on contrastive learning principle, while others like BYOL [20], Barlow Twins [22], etc. use different loss functions to learn representations from the data. Self-supervised contrastive learning treats each data point as a separate class. Thus, a pair made of any two samples constitutes a negative pair. A positive pair of samples is obtained by pairing two augmented versions of a sample. Self-supervised contrastive learning is mainly based on optimizing the InfoNCE [23] loss function. InfoNCE loss in contrastive learning is the same as the categorical cross-entropy loss, but the cosine similarity values between the samples in a pair are treated as logit values. Thus, InfoNCE loss can be considered the negative log of the probability of correctly predicting a positive pair. The main principle behind this learning strategy is to learn an approximate function which maps the feature vector of similar data points closer and dissimilar data points far away. The quality of representation learned by the self-supervised model can be observed from the model’s performance on a linear classification task. But in algorithms like BYOL [20], or Barlow Twins [22], the authors use only the positive pairs for self-supervised representation learning. BYOL [20] optimizes the mean squared error between the feature vectors of the two augmented versions of a sample constituting the positive pair to ensure invariance of representations. Barlow Twins [22] minimizes the cross-correlation between any two feature dimensions under the assumptions that each feature dimension is normally distributed. However, the main challenges of these state-of-the-art algorithms are associated with the experimental configuration, which includes large batch sizes and memory queues, some specific momentum update routine to avoid collapse of representations.

In this paper, we present the contrastive learning scenario as a binary classification problem where each pair is classified as positive or negative. The main contributions of this work can be summarized as follows:

- We propose a novel loss function for contrastive self-supervised learning by modifying the pre-training task as a binary classification problem. We compare the performance of the proposed algorithm to the state-of-the-art (SOTA) self-supervised learning algorithms under the constraints of small input dimensions and short training periods on the task of image classification and the proposed method outperforms the SOTA methods.
- We show that the proposed loss optimizes the mutual information in both positive and negative pairs.
- We present the mathematical form of the gradients of the feature vectors and contribute essential information towards understanding the working principle of the contrastive learning algorithm.
- We also propose an additive  $L_2$  regularizer to our proposed loss function to prevent diverging gradients, which are detrimental to efficient representation learning. We support this proposition by presenting extensive ablation studies on the regularizer.

The rest of the paper is organized as follows: Section 2 describes the proposed methodology. At first it describes the proposed loss function and shows the relation between the mutual information and the proposed loss function. This section also explains the reason for adding a regularizer term based on the gradient of the mapped position of the feature vectors in the feature space. In Section 3, we discuss the details of the experimental configurations that are used to establish the proof of concept. This section also analyzes the performance of the proposed loss function and compares it with the other existing self-supervised algorithms. We present an extensive ablation study to understand the performance of proposed algorithm under different experimental conditions on STL-10 [24] and CIFAR-10 [25] datasets in Section 4. Finally, Section 5 concludes the paper.

## 2 Methodology

In this section, we propose a novel loss function (named MIO-loss) for contrastive learning. For a baseline comparison, we discuss both the proposed loss function and InfoNCE loss [23] and compare the working principle of both the loss functions.

## 2.1 InfoNCE Loss Function

In InfoNCE based contrastive learning framework, each sample is treated as a separate class. The learning principle generally involves maximizing the similarity between two augmented versions of a sample comprising a positive pair and minimizing the similarity between samples in a negative pair. Feature vectors of samples in a positive pair are mapped close to each other in the feature space, whereas feature vectors of samples are pushed away in the case of negative pair. This allows the encoder to learn transformation and context invariant representations such that the feature vectors obtained from samples of different classes are easily separable in the feature space.

The InfoNCE [23] loss function is the negative of the expected log of the probability of correctly predicting the positive pair. The InfoNCE [23] loss function ( $\mathcal{L}_C$ ) is generally used in the form given below

$$\mathcal{L}_C = - \mathbb{E}_{\substack{(x^+, x_k) \sim p_+ \\ (x^+, x_i) \sim p_-}} \left[ \log \frac{e^{\frac{\langle z^+, z_k \rangle}{\tau}}}{e^{\frac{\langle z^+, z_k \rangle}{\tau}} + \sum_{\substack{i=1 \\ i \neq k}}^N e^{\frac{\langle z^+, z_i \rangle}{\tau}}} \right] \quad (1)$$

where  $\langle \cdot, \cdot \rangle$  is the cosine similarity between two feature vectors denoted by  $z$  obtained by passing  $x$  through the encoder and the projector,  $p_+$  and  $p_-$  are the distribution of positive pairs and negative pairs on  $\mathbb{R}^n \times \mathbb{R}^n$ , respectively and  $\tau$  is the temperature parameter.  $(x^+, x_k)$  and  $(x^+, x_i)$  are samples obtained from  $p_+$  and  $p_-$ , respectively,  $x^+$  is the anchor sample. We assume,  $x_+$  and  $x_k$  are obtained by augmenting the  $k$ -th sample in a batch, for simplicity.  $x^+$  forms negative pairs with all samples  $x_i$  (augmented versions of  $i$ -th sample) in the batch, except  $x_k$ .

Assuming  $\tau = 1$ , the above equation can be expressed in the following way:

$$\begin{aligned} \mathcal{L}_C &= - \frac{1}{N} \sum_{j=1}^N \left[ \log \left( \frac{e^{\langle z_j, z_k \rangle}}{e^{\langle z_j, z_k \rangle} + \sum_{\substack{i=1 \\ i \neq k}}^N e^{\langle z_j, z_i \rangle}} \right) \right] \\ &= \frac{1}{N} \sum_{j=1}^N l_j \end{aligned} \quad (2)$$

where

$$l_j = -\log \left( \frac{e^{\langle z_j, z_k \rangle}}{e^{\langle z_j, z_k \rangle} + \sum_{\substack{i=1 \\ i \neq k}}^N e^{\langle z_j, z_i \rangle}} \right) = -\log \left( \frac{e^{C_{jk}}}{e^{C_{jk}} + \sum_{\substack{i=1 \\ i \neq k}}^N e^{C_{ji}}} \right) \quad (3)$$

## 2.2 MIO-loss function

To understand the motivation behind the proposed loss function, let us reiterate the working principle behind contrastive learning. The primary objective of the contrastive learning algorithm is to learn an approximate mapping function that maps the features of the augmented versions of a sample close to each other. For samples belonging to different classes, the feature vectors are mapped as far as possible from each other. The MIO-loss function is based on the fact that there are only two types of pairs in contrastive learning: positive and negative. Hence, the contrastive learning principle can be seen as optimizing the distance between any two samples in the feature space. Thus, the contrastive learning scenario can be morphed into a binary classification problem where a pair of samples is classified either as positive and pulled closer or as negative and pushed apart.

The novel loss function is given below:

$$\mathcal{L}_O = - \mathbb{E}_{(x_i, x_j) \sim p_+} \left[ \log \left( \frac{1}{1 + e^{-\frac{C_{ij}}{\tau}}} \right) \right] - \mathbb{E}_{(x_k, x_l) \sim p_-} \left[ \log \left( 1 - \frac{1}{1 + e^{-\frac{C_{kl}}{\tau}}} \right) \right] \quad (4)$$

where  $p_+$  and  $p_-$  denote the same quantities as described in Sec. 2.1 and  $C_{ij}$  denotes the cosine similarity between the feature vectors  $z_i$  and  $z_j$ .

We follow the same sampling procedure as in SimCLR [17]. Taking a batch size of  $N$ , we augment each sample in the batch to obtain two augmented samples from each sample, forming  $N$  pairs and  $2N$  samples in total. We can form  $4N^2$  pairs in total, out of which  $2N$  are positive pairs and  $2N$  are self-pairs which are discarded. Thus, the total number of negative pairs that can be formed is  $4N^2 - 4N$ . In the figure Fig. 1, we show how the feature vectors are

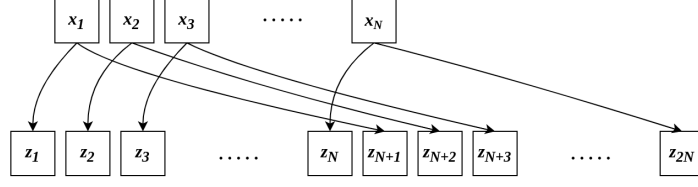


Figure 1: Figure showing how the feature vectors are obtained from the samples  $(x_1, x_2, \dots, x_N)$  in a batch

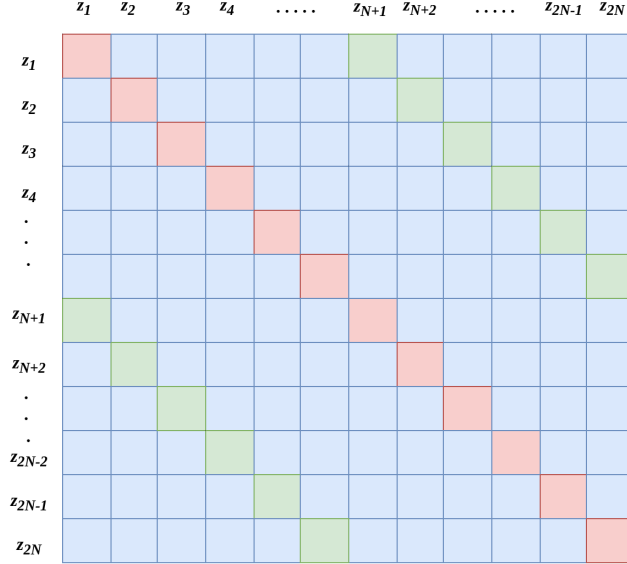


Figure 2: Figure shows how the pairings are obtained. The red cells indicate self-pairs, green cells indicate positive pairs, i.e., pairings between feature vectors of two augmented versions of the same sample, and blue cells indicate negative pairings, i.e. pairings between feature vectors of different samples.

obtained from the samples in a batch and how they are arranged for the final step of calculating the loss. Fig. 2 shows how the different pairs are obtained from the feature vectors.

The MIO-loss can be expressed as follows:

$$\begin{aligned}
 \mathcal{L}_O &= -\frac{1}{T_P} \sum_{(x_i, x_j) \sim \mathcal{X}_+} \log \left( \frac{1}{1 + e^{-\frac{c_{ij}}{\tau}}} \right) - \frac{1}{T_N} \sum_{(x_k, x_l) \sim \mathcal{X}_-} \log \left( 1 - \frac{1}{1 + e^{-\frac{c_{kl}}{\tau}}} \right) \\
 &= -\frac{1}{T_P} \sum_{j=1}^{T_P} \left[ \log \left( \frac{1}{1 + e^{-\frac{c_{jk}}{\tau}}} \right) + \frac{1}{T_P - 2} \sum_{\substack{i=1 \\ i \neq j, k}}^{T_P} \log \left( 1 - \frac{1}{1 + e^{-\frac{c_{ji}}{\tau}}} \right) \right] \tag{5}
 \end{aligned}$$

where  $T_P = 2N$  and  $T_N = 4N^2 - 4N$ . We can deduce a small relation between  $T_P$  and  $T_N$  and can be stated as  $T_N = T_P^2 - 2T_P$ .  $\mathcal{X}_+$  and  $\mathcal{X}_-$  denote the sets obtained from sampling pairs from the distributions  $p_+$  and  $p_-$  in a single batch iteration, respectively.

### 2.3 Relation of MIO-loss and Mutual Information

In this subsection, we are going to derive the relationship between the MIO-loss function and mutual information [26, 27, 28] between the samples in a pair. The final expression of the lower bound of the MIO-loss function will allow us to visualize the optimization process intuitively.

Let us define the scoring function

$$h(z_i, z_j) = e^{C_{ij}} \quad (6)$$

where  $C_{ij}$  is the cosine similarity between  $z_i$  and  $z_j$ .

Now, the probability of the pair  $(z_i, z_j)$  being a positive pair in a binary classification setting can be expressed as:

$$P(\text{pos} = 1 | (z_i, z_j)) = \frac{P_+(z_i, z_j)}{P_+(z_i, z_j) + P_-(z_i, z_j)} \quad (7)$$

Here,  $P_+(z_i, z_j)$  is the probability of obtaining the positive pair  $(z_i, z_j)$  and  $P_-(z_i, z_j)$  is the probability of obtaining the negative pair  $(z_i, z_j)$ . In Fig. 3, the positive transformed pair  $(z_1, z_2)$  is obtained from the same sample  $z$ . Considering  $p_Z(z_1)$  as the probability of obtaining  $z_1$  from the distribution  $p_Z$  over all possible transformed samples  $z_i$  and  $p_{Z,Z}(z_1, z_2)$  as the probability of obtaining  $(z_1, z_2)$  from the joint distribution  $p_{Z,Z}$ , we deduce the following relations. Since,  $z$  is not observed, we cannot consider  $z_1$  and  $z_2$  as independent. Thus,  $P_+(z_1, z_2)$  is equal to the probability  $p_{Z,Z}(z_1, z_2)$ . However, when considering  $(z_1, z_2)$  as negative transformed pair, there will be no dependency between the two samples. Thus,  $z_1$  and  $z_2$  can be considered independent and  $P_-(z_1, z_2)$  can be considered as the product of  $p_Z(z_1)$  and  $p_Z(z_2)$ .

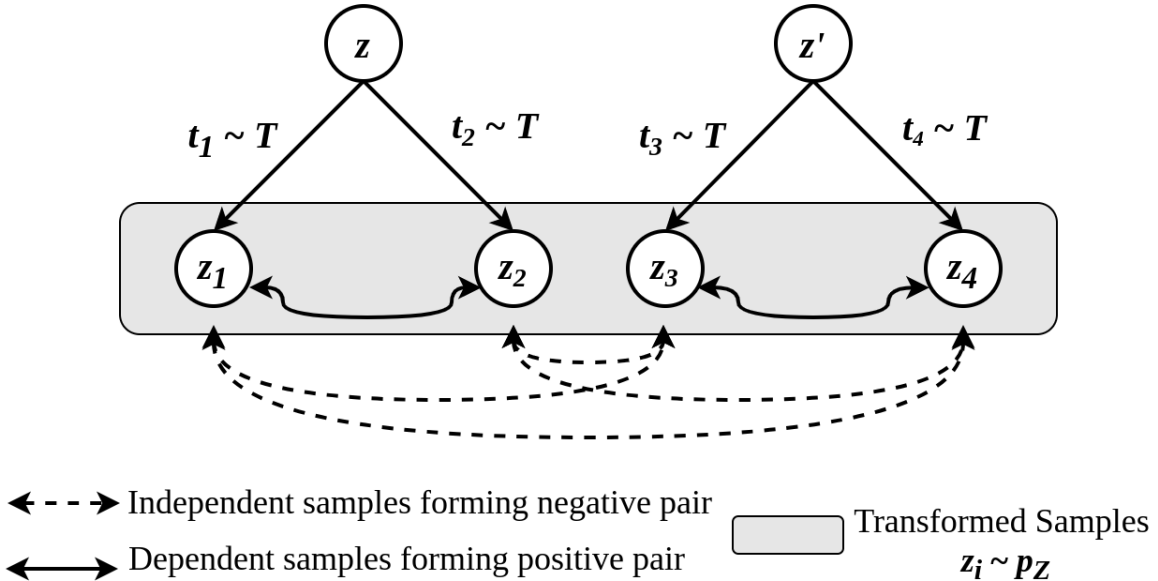


Figure 3: Graphical Model [29] showing the dependency between two samples in a positive pair and the independency between two samples forming negative pair. Here,  $z$  and  $z'$  are two different samples in a dataset.  $t_1, t_2, t_3, t_4$  are randomly chosen transformations from the distribution  $T$ .  $z_1$  and  $z_2$  are obtained by applying  $t_1$  and  $t_2$  on  $z$ .  $z_3$  and  $z_4$  are obtained by applying  $t_3$  and  $t_4$  on  $z'$ .

Therefore, using the same idea, Eq. (7) can be expanded as follows:

$$P(\text{pos} = 1 | (z_i, z_j)) = \frac{p_{Z,Z}(z_i, z_j)}{p_Z(z_i)p_Z(z_j) + p_{Z,Z}(z_i, z_j)} = \frac{\frac{p_{Z,Z}(z_i, z_j)}{p_Z(z_i)p_Z(z_j)}}{1 + \frac{p_{Z,Z}(z_i, z_j)}{p_Z(z_i)p_Z(z_j)}} \quad (8)$$

We can also express  $p(pos = 1|(z_i, z_j))$  in terms of  $h(z_i, z_j)$  as follows

$$P(pos = 1|(z_i, z_j)) = \frac{h(z_i, z_j)}{1 + h(z_i, z_j)} \quad (9)$$

Thus, comparing Eq. (8) and Eq. (9), we get,

$$h(z_i, z_j) = e^{\langle z_i, z_j \rangle} = \frac{p_{Z,Z}(z_i, z_j)}{p_Z(z_i)p_Z(z_j)} \quad (10)$$

Putting Eq. (10) in Eq. (4), we get,

$$\begin{aligned} \mathcal{L}_O &= - \mathbb{E}_{(x_i, x_j) \sim p_+} \left[ \log \left( \frac{\frac{p_{Z,Z}(z_i, z_j)}{p_Z(z_i)p_Z(z_j)}}{1 + \frac{p_{Z,Z}(z_i, z_j)}{p_Z(z_i)p_Z(z_j)}} \right) \right] - \mathbb{E}_{(x_i, x_j) \sim p_-} \left[ \log \left( \frac{1}{1 + \frac{p_{Z,Z}(z_k, z_l)}{p_Z(z_k)p_Z(z_l)}} \right) \right] \\ &\geq - \mathbb{E}_{(x_i, x_j) \sim p_+} \left[ \log \left( \frac{p_{Z,Z}(z_i, z_j)}{p_Z(z_i)p_Z(z_j)} \right) \right] + \mathbb{E}_{(x_i, x_j) \sim p_-} \left[ \log \left( \frac{p_{Z,Z}(z_k, z_l)}{p_Z(z_k)p_Z(z_l)} \right) \right] \\ &\geq - \mathcal{I}_{(z_i, z_j) \sim p_+} (z_i, z_j) + \mathcal{I}_{(z_k, z_l) \sim p_-} (z_k, z_l) \end{aligned} \quad (11)$$

From Eq. (11), we can infer that the proposed loss function  $\mathcal{L}_O$  works by maximizing the mutual information between the samples in a positive pair  $(z_i, z_j)$ . It also minimizes the mutual information between the samples in a negative pair  $(z_k, z_l)$ .

An intuitive explanation behind the working principle of the MIO-loss function is that when the samples in a negative pair belong to the same underlying category, the encoder learns only the common representations between them, including both low and high-level representations. The mutual information is the least when the two samples in a negative pair belong to two different classes. In that case, the encoder should learn only the common low-level representations among all the samples in the dataset. High-level representations are better learned when the mutual information is maximized for samples in a positive pair.

## 2.4 Analysis of the Proposed MIO-loss

In this subsection, we are going to analyze the gradients of the MIO-loss function, which flow into the projector of the self-supervised model. For the analysis we consider the self-supervised model consisting of an encoder and a non-linear projector. Let the input, encoder, encoder output (projector input), projector and the final feature vector be denoted by  $x, f, h, q$ , and  $z$ , respectively. The input images  $x \in \mathbb{R}^H \times \mathbb{R}^W \times \mathbb{R}^C$  when passed through the encoder  $f$ , a latent vector  $h \in \mathbb{R}^F$  is obtained. This latent vector  $h$  gives the final feature vector  $z \in \mathbb{R}^D$  when passed through the projector  $q$ . The loss function  $\mathcal{L}_O$  takes the feature vectors and outputs a scalar  $\mathcal{L} \in \mathbb{R}^1$ .

To understand the flow of information we can devise the following equations

$$z = q(h) = q(f(x)) \quad (12)$$

### 2.4.1 Derivation of Gradient Flowing into the Projector for the Proposed Loss Function

For a 2-layered non-linear projector  $q$ , we can express it as  $q_w = W^1 \cdot W^2$ , where  $W^1$  and  $W^2$  are the parameters of the two layers in  $q$ , with dimensions  $F \times F$  and  $F \times D$ , respectively. Without loss of generality, we are not considering batch normalization and biases. Thus,  $z = q(f(x)) = h \cdot q_w = h \cdot (W^1 \cdot W^2)$ . Thus,  $q(u) = u \cdot (W_q^2) \cdot (W_q^1)$ . Differentiating the loss with respect to  $q_w$ , we obtain the gradients, which get distributed to the hidden layer perceptrons from each output perceptron of the projector. This explains why we obtained the gradient of the dimension  $1 \times D$  in Eq. (20). Now,  $z = q(h) = q(f(x))$ . Therefore,

$$\frac{\partial}{\partial q_w} q(f(x)) = \frac{\partial}{\partial ((W_q^2) \cdot (W_q^1))} (f(x) \cdot (W_q^2) \cdot (W_q^1)) = f(x) = h \quad (13)$$

$$\frac{\partial}{\partial q_w} q(f(x))_m = \frac{\partial}{\partial ((W_q^2) \cdot (W_q^1))} (f(x) \cdot (W_q^2)_{(:,m)} \cdot (W_q^1)) \quad (14)$$

Continuing from Eqn.14,

$$\begin{aligned} \frac{\partial((W_q^2)^{(:,m)} \cdot (W_q^1))}{\partial((W_q^2) \cdot (W_q^1))} &= \left[ \frac{\partial((W_q^2)^{(:,m)} \cdot (W_q^1))}{\partial((W_q^2)^{(:,1)} \cdot (W_q^1))}, \dots, \frac{\partial((W_q^2)^{(:,m)} \cdot (W_q^1))}{\partial((W_q^2)^{(:,m)} \cdot (W_q^1))}, \frac{\partial((W_q^2)^{(:,m)} \cdot (W_q^1))}{\partial((W_q^2)^{(:,m+1)} \cdot (W_q^1))}, \dots, \frac{\partial((W_q^2)^{(:,m)} \cdot (W_q^1))}{\partial((W_q^2)^{(:,D)} \cdot (W_q^1))} \right] \\ &= [\mathbf{0}^T, \dots, \mathbf{1}^T, \mathbf{0}^T, \dots, \mathbf{0}^T]_{F \times D} \end{aligned} \quad (15)$$

The outcome of Eqn.15 is a matrix with dimensions  $F \times D$  and with the  $m$ -th column with all 1s. This when multiplied to  $f(x)$  of dimensions  $N \times F$ , gives an output with dimensions  $N \times D$  with only the  $m$ -th element being non-zero. Thus,

$$\begin{aligned} \frac{\partial}{\partial q_w} q(f(x))_m &= \frac{\partial}{\partial((W_q^2) \cdot (W_q^1))} (f(x) \cdot (W_q^2)^{(:,m)} \cdot (W_q^1)) \\ &= f(x) \frac{\partial((W_q^2)^{(:,m)} \cdot (W_q^1))}{\partial((W_q^2) \cdot (W_q^1))} \\ &= f(x) \cdot [\mathbf{0}^T, \dots, \mathbf{1}^T, \mathbf{0}^T, \dots, \mathbf{0}^T]_{F \times D} = [0, \dots, \sum_t^F h_t, 0, \dots, 0]_{1 \times D} \end{aligned} \quad (16)$$

Differentiating  $e^{C_{jk}}$  with respect to  $q_w$ , we get,

$$\begin{aligned} \frac{\partial}{\partial q_w} e^{C_{jk}} &= \frac{\partial}{\partial q_w} e^{\langle q(f(x_j)), q(f(x_k)) \rangle} \\ &= e^{\langle q(f(x_j)), q(f(x_k)) \rangle} \frac{\partial}{\partial q_w} \sum_{m=1}^D q(f(x_j))_m \cdot q(f(x_k))_m \\ &= e^{\langle q(f(x_j)), q(f(x_k)) \rangle} \sum_{m=1}^D \frac{\partial}{\partial q_w} (q(f(x_j))_m \cdot q(f(x_k))_m) \\ &= e^{\langle q(f(x_j)), q(f(x_k)) \rangle} \sum_{m=1}^D \left( q(f(x_j))_m \cdot \frac{\partial}{\partial q_w} q(f(x_k))_m + q(f(x_k))_m \cdot \frac{\partial}{\partial q_w} q(f(x_j))_m \right) \\ &= e^{C_{jk}} \sum_{m=1}^D \left( (z_j)_m \cdot \frac{\partial}{\partial q_w} q(h_k)_m + (z_k)_m \cdot \frac{\partial}{\partial q_w} (z_j)_m \right) \\ &= e^{C_{jk}} \sum_{m=1}^D \left( (z_j)_m \cdot [0, \dots, \sum_t^F (h_k)_t, 0, \dots, 0] + q(h_k)_m \cdot [0, \dots, \sum_t^F (h_j)_t, 0, \dots, 0] \right) \\ &= e^{C_{jk}} \sum_{m=1}^D \left( [0, \dots, (z_j)_m \cdot \sum_t^F (h_k)_t, 0, \dots, 0] + [0, \dots, q(h_k)_m \cdot \sum_t^F (h_j)_t, 0, \dots, 0] \right) \\ &= e^{C_{jk}} \sum_{m=1}^D [0, \dots, \left( (z_j)_m \cdot \sum_{u=1}^F (h_k)_u + q(h_k)_m \cdot \sum_{u=1}^F (h_j)_u \right), 0, \dots, 0]_{1 \times D} \\ &= e^{C_{jk}} \begin{bmatrix} (z_j)_1 \cdot \sum_{u=1}^F (h_k)_u + q(h_k)_1 \cdot \sum_{u=1}^F (h_j)_u \\ (z_j)_2 \cdot \sum_{u=1}^F (h_k)_u + q(h_k)_2 \cdot \sum_{u=1}^F (h_j)_u \\ \vdots \\ (z_j)_m \cdot \sum_{u=1}^F (h_k)_u + q(h_k)_m \cdot \sum_{u=1}^F (h_j)_u \\ \vdots \\ (z_j)_{D-1} \cdot \sum_{u=1}^F (h_k)_u + q(h_k)_{D-1} \cdot \sum_{u=1}^F (h_j)_u \\ (z_j)_D \cdot \sum_{u=1}^F (h_k)_u + q(h_k)_D \cdot \sum_{u=1}^F (h_j)_u \end{bmatrix}_{D \times 1} \end{aligned} \quad (17)$$

Let us define,

$$Q_{jk}^h = \begin{bmatrix} (z_j)_1 \cdot \sum_{u=1}^F (h_k)_u + q(h_k)_1 \cdot \sum_{u=1}^F (h_j)_u \\ (z_j)_2 \cdot \sum_{u=1}^F (h_k)_u + q(h_k)_2 \cdot \sum_{u=1}^F (h_j)_u \\ \vdots \\ (z_j)_m \cdot \sum_{u=1}^F (h_k)_u + q(h_k)_m \cdot \sum_{u=1}^F (h_j)_u \\ \vdots \\ (z_j)_{D-1} \cdot \sum_{u=1}^F (h_k)_u + q(h_k)_{D-1} \cdot \sum_{u=1}^F (h_j)_u \\ (z_j)_D \cdot \sum_{u=1}^F (h_k)_u + q(h_k)_D \cdot \sum_{u=1}^F (h_j)_u \end{bmatrix}_{D \times 1}^T = \begin{bmatrix} (z_j)_1 \cdot \|h_k\|_1 + q(h_k)_1 \cdot \|h_j\|_1 \\ (z_j)_2 \cdot \|h_k\|_1 + q(h_k)_2 \cdot \|h_j\|_1 \\ \vdots \\ (z_j)_m \cdot \|h_k\|_1 + q(h_k)_m \cdot \|h_j\|_1 \\ \vdots \\ (z_j)_{D-1} \cdot \|h_k\|_1 + q(h_k)_{D-1} \cdot \|h_j\|_1 \\ (z_j)_D \cdot \|h_k\|_1 + q(h_k)_D \cdot \|h_j\|_1 \end{bmatrix}_{D \times 1}^T \quad (18)$$

This quantity  $Q_{jk}^h$  can be described as the Influence factor of the pair  $(x_j, x_k)$  on the gradient. The gradient can be described as the negative of the average of a quantity which is the sum of the Influence of the positive pair weighted by the prediction error and the average of Influence of the negative pairs, where each term is weighted by the respective prediction error. As the encoder learns a better approximation of the mapping function from the input to the feature space, the prediction errors will decrease and the contribution of the Influence terms will also decrease.

[Assuming, the encoder  $f$  has ReLU as its last layer,  $h_i \geq 0 \forall i \forall h$ ]

The derivative of the proposed loss function with respect to  $q_w$ , that is the parameters of the projector  $q$ , is given by

$$\begin{aligned} \frac{\partial \mathcal{L}_O}{\partial q_w} &= \frac{\partial}{\partial q_w} \left[ -\frac{1}{T_P} \sum_{j=1}^{T_P} \left[ \log \left( \frac{1}{1 + e^{-\frac{C_{jk}}{\tau}}} \right) + \frac{1}{T_P - 2} \sum_{\substack{i=1 \\ i \neq j, k}}^{T_P} \log \left( 1 - \frac{1}{1 + e^{-\frac{C_{ji}}{\tau}}} \right) \right] \right] \\ &= -\frac{1}{T_P} \sum_{j=1}^{T_P} \left[ \frac{\partial}{\partial q_w} \log \left( \frac{1}{1 + e^{-\frac{C_{jk}}{\tau}}} \right) + \frac{1}{T_P - 2} \sum_{\substack{i=1 \\ i \neq j, k}}^{T_P} \frac{\partial}{\partial q_w} \log \left( 1 - \frac{1}{1 + e^{-\frac{C_{ji}}{\tau}}} \right) \right] \\ &= -\frac{1}{T_P} \sum_{j=1}^{T_P} \left[ \frac{\frac{\partial}{\partial q_w} \left( \frac{1}{1 + e^{-\frac{C_{jk}}{\tau}}} \right)}{\frac{1}{1 + e^{-\frac{C_{jk}}{\tau}}}} - \frac{1}{T_P - 2} \sum_{\substack{i=1 \\ i \neq j, k}}^{T_P} \frac{\frac{\partial}{\partial q_w} \left( 1 - \frac{1}{1 + e^{-\frac{C_{ji}}{\tau}}} \right)}{1 - \frac{1}{1 + e^{-\frac{C_{ji}}{\tau}}}} \right] \\ &= -\frac{1}{T_P} \sum_{j=1}^{T_P} \left[ \frac{\frac{1}{\left( 1 + e^{-\frac{C_{jk}}{\tau}} \right)^2} \frac{\partial}{\partial q_w} \left( 1 + e^{-\frac{C_{jk}}{\tau}} \right)}{\frac{1}{1 + e^{-\frac{C_{jk}}{\tau}}}} - \frac{1}{T_P - 2} \sum_{\substack{i=1 \\ i \neq j, k}}^{T_P} \frac{\frac{1}{\left( 1 + e^{-\frac{C_{ji}}{\tau}} \right)^2} \frac{\partial}{\partial q_w} \left( 1 + e^{-\frac{C_{ji}}{\tau}} \right)}{1 - \frac{1}{1 + e^{-\frac{C_{ji}}{\tau}}}} \right] \\ &= -\frac{1}{T_P} \sum_{j=1}^{T_P} \left[ \frac{\frac{\partial}{\partial q_w} \left( 1 + e^{-\frac{C_{jk}}{\tau}} \right)}{1 + e^{-\frac{C_{jk}}{\tau}}} - \frac{1}{T_P - 2} \sum_{\substack{i=1 \\ i \neq j, k}}^{T_P} \frac{\frac{\partial}{\partial q_w} \left( 1 + e^{-\frac{C_{ji}}{\tau}} \right)}{e^{-\frac{C_{ji}}{\tau}} \left( 1 + e^{-\frac{C_{ji}}{\tau}} \right)} \right] \\ &= -\frac{1}{T_P} \sum_{j=1}^{T_P} \left[ \frac{e^{-\frac{C_{jk}}{\tau}} \frac{\partial}{\partial q_w} \left( -\frac{C_{jk}}{\tau} \right)}{1 + e^{-\frac{C_{jk}}{\tau}}} - \frac{1}{T_P - 2} \sum_{\substack{i=1 \\ i \neq j, k}}^{T_P} \frac{e^{-\frac{C_{ji}}{\tau}} \frac{\partial}{\partial q_w} \left( -\frac{C_{ji}}{\tau} \right)}{e^{-\frac{C_{ji}}{\tau}} \left( 1 + e^{-\frac{C_{ji}}{\tau}} \right)} \right] \\ &= -\frac{1}{T_P} \sum_{j=1}^{T_P} \left[ \frac{\frac{\partial}{\partial q_w} \left( -\frac{C_{jk}}{\tau} \right)}{e^{\frac{C_{jk}}{\tau}} \left( 1 + e^{-\frac{C_{jk}}{\tau}} \right)} - \frac{1}{T_P - 2} \sum_{\substack{i=1 \\ i \neq j, k}}^{T_P} \frac{\frac{\partial}{\partial q_w} \left( -\frac{C_{ji}}{\tau} \right)}{\left( 1 + e^{-\frac{C_{ji}}{\tau}} \right)} \right] \\ &= -\frac{1}{T_P} \sum_{j=1}^{T_P} \left[ \frac{\frac{\partial}{\partial q_w} \left( -\frac{C_{jk}}{\tau} \right)}{e^{\frac{C_{jk}}{\tau}} \left( 1 + e^{-\frac{C_{jk}}{\tau}} \right)} - \frac{1}{T_P - 2} \sum_{\substack{i=1 \\ i \neq j, k}}^{T_P} \frac{\frac{\partial}{\partial q_w} \left( -\frac{C_{ji}}{\tau} \right)}{\left( 1 + e^{-\frac{C_{ji}}{\tau}} \right)} \right] \end{aligned}$$



$$\begin{aligned}
&= -\frac{1}{T_P} \sum_{j=1}^{T_P} \left[ \frac{\mathcal{Q}_{ij}^h}{e^{\frac{C_{jk}}{\tau}} \left(1 + e^{-\frac{C_{jk}}{\tau}}\right)} - \frac{1}{T_P - 2} \sum_{\substack{i=1 \\ i \neq j, k}}^{T_P} \frac{\mathcal{Q}_{kl}^h}{\left(1 + e^{-\frac{C_{ji}}{\tau}}\right)} \right] \\
&= -\frac{1}{T_P} \sum_{j=1}^{T_P} \left[ \frac{\mathcal{Q}_{ij}^h}{1 + e^{\frac{C_{jk}}{\tau}}} - \frac{1}{T_P - 2} \sum_{\substack{i=1 \\ i \neq j, k}}^{T_P} \frac{e^{\frac{C_{ji}}{\tau}} \mathcal{Q}_{kl}^h}{\left(1 + e^{\frac{C_{ji}}{\tau}}\right)} \right] \\
&= -\frac{1}{T_P} \sum_{j=1}^{T_P} \left[ \left(1 - \frac{1}{1 + e^{-\frac{C_{jk}}{\tau}}}\right) \mathcal{Q}_{jk}^h - \frac{1}{T_P - 2} \sum_{\substack{i=1 \\ i \neq k, j}}^{T_P} \left(\frac{1}{1 + e^{-\frac{C_{ji}}{\tau}}}\right) \mathcal{Q}_{ji}^h \right] \\
&= -\frac{1}{T_P} \sum_{j=1}^{T_P} \left[ \left(1 - \frac{1}{1 + e^{-\frac{C_{jk}}{\tau}}}\right) \mathcal{Q}_{jk}^h + \frac{1}{T_P - 2} \sum_{\substack{i=1 \\ i \neq k, j}}^{T_P} \left(0 - \frac{1}{1 + e^{-\frac{C_{ji}}{\tau}}}\right) \mathcal{Q}_{ji}^h \right]
\end{aligned} \tag{19}$$

Assuming  $\tau = 1.0$  without loss of generality and applying the same to the above equation, we get,

$$\frac{\partial \mathcal{L}_O}{\partial q_w} = -\frac{1}{T_P} \sum_{j=1}^{T_P} \left[ \left(1 - \frac{1}{1 + e^{-C_{jk}}}\right) \mathcal{Q}_{jk}^h + \frac{1}{T_P - 2} \sum_{\substack{i=1 \\ i \neq k, j}}^{T_P} \left(0 - \frac{1}{1 + e^{-C_{ji}}}\right) \mathcal{Q}_{ji}^h \right] \tag{20}$$

## 2.4.2 Derivation of Gradient Flowing into the Projector for the InfoNCE Loss Function

When using the InfoNCE [23] loss function the total gradient that flows into the hidden layer perceptrons of the projector  $q$  can be calculated in a similar way as Eq. (20). Differentiating the above Eq. (3) with respect to  $q_w$ , we get,

$$\begin{aligned}
\frac{\partial l_j}{\partial q_w} &= -\frac{\partial}{\partial q_w} \left[ \log \left( \frac{e^{C_{jk}}}{e^{C_{jk}} + \sum_{\substack{i=1 \\ i \neq k, j}}^N e^{C_{ji}}} \right) \right] \\
&= -\frac{\partial}{\partial q_w} \left[ \log \left( \frac{e^{C_{jk}}}{\sum_{\substack{i=1 \\ i \neq j}}^N e^{C_{ji}}} \right) \right] \\
&= \frac{e^{C_{jk}} \frac{\partial}{\partial q_w} \left( \sum_{\substack{i=1 \\ i \neq j}}^N e^{C_{ji}} \right) - \left( \sum_{\substack{i=1 \\ i \neq j}}^N e^{C_{ji}} \right) \frac{\partial}{\partial q_w} e^{C_{jk}}}{\left( \sum_{\substack{i=1 \\ i \neq j}}^N e^{C_{ji}} \right)^2} \\
&= \frac{\left( \frac{e^{C_{jk}}}{\sum_{\substack{i=1 \\ i \neq j}}^N e^{C_{ji}}} \right)}{\left( \sum_{\substack{i=1 \\ i \neq j}}^N e^{C_{ji}} \right)} \\
&= \frac{e^{C_{jk}} \frac{\partial}{\partial q_w} \left( \sum_{\substack{i=1 \\ i \neq j}}^N e^{C_{ji}} \right) - \left( \sum_{\substack{i=1 \\ i \neq j}}^N e^{C_{ji}} \right) \frac{\partial}{\partial q_w} e^{C_{jk}}}{e^{C_{jk}} \left( \sum_{\substack{i=1 \\ i \neq j}}^N e^{C_{ji}} \right)} \\
&= \frac{e^{C_{jk}} \frac{\partial}{\partial q_w} \left( \sum_{\substack{i=1 \\ i \neq j}}^N e^{C_{ji}} \right) - \left( \sum_{\substack{i=1 \\ i \neq j}}^N e^{C_{ji}} \right) \frac{\partial}{\partial q_w} e^{C_{jk}}}{e^{C_{jk}} \left( \sum_{\substack{i=1 \\ i \neq j}}^N e^{C_{ji}} \right)}
\end{aligned}$$

$$\begin{aligned}
&= \frac{e^{C_{jk}} (\sum_{i=1}^N e^{C_{ji}} \mathcal{Q}_{ji}^h) - (\sum_{i=1}^N e^{C_{ji}}) e^{C_{jk}} \mathcal{Q}_{jk}^h}{e^{\langle z_j, q(h_k) \rangle} (\sum_{i=1}^N e^{C_{ji}})} \\
&= \frac{(\sum_{i=1}^N e^{C_{ji}} \mathcal{Q}_{ji}^h) - (\sum_{i=1}^N e^{\langle z_j, z_i \rangle}) \mathcal{Q}_{jk}^h}{(\sum_{i=1}^N e^{C_{ji}})} \\
&= - \left[ \mathcal{Q}_{jk}^h - \frac{(\sum_{i=1}^N e^{C_{ji}} \mathcal{Q}_{ji}^h)}{(\sum_{i=1}^N e^{C_{ji}})} \right] \tag{21}
\end{aligned}$$

The final expression for the gradient of the InfoNCE loss with respect to  $q_w$ ,

$$\frac{\partial \mathcal{L}_C}{\partial q_w} = \frac{1}{N} \sum_{j=1}^N l_j = -\frac{1}{N} \sum_{j=1}^N \left[ \mathcal{Q}_{jk}^h - \frac{(\sum_{i=1}^N e^{C_{ji}} \mathcal{Q}_{ji}^h)}{(\sum_{i=1}^N e^{C_{ji}})} \right] \tag{22}$$

### 2.4.3 Displacement of the feature vector $z_o$ when using MIO-loss

In this subsection, we present the gradient of the loss with respect to the feature vector, which gives a simple idea about the locus of a particular feature vector  $z_o$  with respect to the other feature vectors in the feature space. Eq. (5) gives the expression for the MIO-loss function in a form such that it is convenient to obtain the gradients similar to the InfoNCE [23] loss function. Considering  $(z_o, z_{o'})$  forms the positive pair and differentiating  $\mathcal{L}_O$  with respect to  $z_o$ , we get,

$$\begin{aligned}
\frac{\partial \mathcal{L}_O}{\partial z_o} &= -\frac{1}{T_P} \sum_{j=1}^{T_P} \left[ -\frac{\partial}{\partial z_o} \log(1 + e^{-C_{oo'}}) + \frac{1}{T_P - 2} \sum_{\substack{i=1 \\ i \neq o, o'}}^{T_P} \frac{\partial}{\partial z_o} [\log(e^{-C_{oi}}) - \log(1 + e^{-C_{oi}})] \right] \\
&= -\frac{1}{T_P} \left[ -\frac{z_{o'} \cdot e^{-C_{oo'}}}{1 + e^{-C_{oo'}}} + \frac{1}{T_P - 2} \sum_{\substack{i=1 \\ i \neq o, o'}}^{T_P} \left[ -z_i - \frac{-z_i \cdot e^{-C_{oi}}}{1 + e^{-C_{oi}}} \right] \right] \\
&= -\frac{1}{T_P} \left[ \frac{z_{o'} \cdot e^{-C_{oo'}}}{1 + e^{-C_{oo'}}} - \frac{1}{T_P - 2} \sum_{\substack{i=1 \\ i \neq o, o'}}^{T_P} \left[ \frac{z_i}{1 + e^{-C_{oi}}} \right] \right] \\
&= -\frac{1}{T_P} \left[ z_{o'} - \frac{z_{o'}}{1 + e^{-C_{oo'}}} - \frac{1}{T_P - 2} \sum_{\substack{i=1 \\ i \neq o, o'}}^{T_P} \left[ \frac{z_i}{1 + e^{-C_{oi}}} \right] \right] \\
&= -\frac{1}{T_P} \left[ z_{o'} - \left[ \frac{z_{o'}}{1 + e^{-C_{oo'}}} + \frac{1}{T_P - 2} \sum_{\substack{i=1 \\ i \neq o, o'}}^{T_P} \left[ \frac{z_i}{1 + e^{-C_{oi}}} \right] \right] \right] \\
&= -\frac{1}{T_P} \left[ z_{o'} - \left[ p_+(o, o') \cdot z_{o'} + \frac{1}{T_P - 2} \sum_{\substack{i=1 \\ i \neq o, o'}}^{T_P} p_+(o, i) \cdot z_i \right] \right] \\
&= -\frac{1}{T_P} \left[ z_{o'} \cdot (1 - p_+(o, o')) - \frac{1}{T_P - 2} \sum_{\substack{i=1 \\ i \neq o, o'}}^{T_P} z_i \cdot p_+(o, i) \right]
\end{aligned}$$

$$= -\frac{1}{T_P} \left[ z_{o'} \cdot (1 - p_+(o, o')) + \frac{1}{T_P - 2} \sum_{\substack{i=1 \\ i \neq o, o'}}^{T_P} z_i \cdot (0 - p_+(o, i)) \right] \quad (23)$$

where  $C_{ji}$  and  $p_+(j, i)$  are defined earlier.

From the above Eq. (23), we can deduce that the displacement of the feature vector  $z_o$  assumes a form similar to the gradient of the loss function with respect to  $q_w$ , given by Eq. (19) in Sec. 2.4.1. The displacement of the feature vectors can be expressed as the negative weighted sum of two terms. The first term is the feature vector of the second sample  $z_{o'}$  in the positive pair weighted by the prediction error. The second term is the average of the feature vectors of the samples with which  $x_o$  forms negative pairs, weighted by the respective prediction errors.

Since,  $C_{oo'}$  and  $C_{o'o}$  are essentially the same pair and the other pairing in  $C_{oi}$  are all in separate terms, the calculation of the displacement of  $z_o$  is a lot simpler than the displacement of  $z_o$  when using InfoNCE loss, as shown in Sec. 2.4.4.

#### 2.4.4 Displacement of the feature vector $z_o$ when using the InfoNCE loss

Calculating the displacement of  $z_o$  when using the InfoNCE loss also follows the same procedure as follows. However, as in InfoNCE loss, we basically use categorical cross-entropy loss, we will need to consider the terms where  $z_o$  is present in the denominator as a negative pairing as well. Here, we consider  $z_j$  and  $z_k$  to be obtained from the same parent samples by augmentations and form the positive pair.

Differentiating any  $l_i$  in Eq. (3) with respect to  $z_o$ , we get,

$$\begin{aligned} \frac{\partial l_j}{\partial z_o} &= -\frac{\partial}{\partial z_o} \log \left( \frac{e^{C_{jk}}}{e^{C_{jk}} + \sum_{\substack{i=1 \\ i \neq j}}^N e^{C_{ji}}} \right) \\ &= -\frac{\partial}{\partial z_o} \left[ C_{jk} - \log \left( e^{C_{jk}} + \sum_{\substack{i=1 \\ i \neq j}}^N e^{C_{ji}} \right) \right] \\ &= -\frac{\partial}{\partial z_o} \left[ C_{jk} - \log \left( e^{C_{jk}} + \sum_{\substack{i=1 \\ i \neq j, o}}^N e^{C_{ji}} + e^{C_{jo}} \right) \right] \\ &= \frac{\frac{\partial}{\partial z_o} e^{C_{jo}}}{e^{C_{jk}} + \sum_{\substack{i=1 \\ i \neq j, o}}^N e^{C_{ji}} + e^{C_{jo}}} \\ &= \frac{z_j \cdot e^{C_{jo}}}{e^{C_{jk}} + \sum_{\substack{i=1 \\ i \neq j}}^N e^{C_{ji}}} \end{aligned} \quad (24)$$

Now, let us differentiate  $l_o$  with  $z_o$  as anchor sample with respect to the same. Let us consider  $z_{o'}$  as the other sample in the positive pair. Differentiating  $l_o$  with respect to  $z_o$ , we get,

$$\begin{aligned}
\frac{\partial l_o}{\partial z_o} &= -\frac{\partial}{\partial z_o} \log \left( \frac{e^{C_{oo'}}}{e^{C_{oo'}} + \sum_{\substack{i=1 \\ i \neq k}}^N e^{C_{oi}}} \right) \\
&= -\frac{\partial}{\partial z_o} \left[ C_{oo'} - \log \left( e^{C_{oo'}} + \sum_{\substack{i=1 \\ i \neq k}}^N e^{C_{oi}} \right) \right] \\
&= -\frac{\partial}{\partial z_o} \left[ C_{oo'} - \log \left( e^{C_{oo'}} + \sum_{\substack{i=1 \\ i \neq o}}^N e^{C_{oi}} \right) \right] \\
&= -\frac{\partial}{\partial z_o} C_{oo'} + \frac{\frac{\partial}{\partial z_o} e^{C_{oo'}} + \frac{\partial}{\partial z_o} \sum_{\substack{i=1 \\ i \neq o}}^N e^{C_{oi}}}{e^{C_{oo'}} + \sum_{\substack{i=1 \\ i \neq o}}^N e^{C_{oi}}} \\
&= -z_{o'} + \frac{z_{o'} \cdot e^{C_{oo'}} + \sum_{\substack{i=1 \\ i \neq o}}^N z_i \cdot e^{C_{oi}}}{e^{C_{oo'}} + \sum_{\substack{i=1 \\ i \neq o}}^N e^{C_{oi}}}
\end{aligned} \tag{25}$$

The total displacement of the vector  $z_o$  is equal to  $\frac{\partial \mathcal{L}}{\partial z_o}$ , where  $\mathcal{L}$  is given by Eq. (2).

$$\begin{aligned}
\frac{\partial \mathcal{L}_C}{\partial z_o} &= \frac{1}{N} \sum_{j=1}^N \frac{\partial l_j}{\partial z_o} \\
&= \frac{1}{N} \left[ \frac{\partial l_o}{\partial z_o} + \sum_{\substack{j=1 \\ j \neq o}}^N \frac{\partial l_j}{\partial z_o} \right] \\
&= \frac{1}{N} \left[ -z_{o'} + \frac{z_{o'} \cdot e^{C_{oo'}} + \sum_{\substack{i=1 \\ i \neq o}}^N z_i \cdot e^{C_{oi}}}{e^{C_{oo'}} + \sum_{\substack{i=1 \\ i \neq o}}^N e^{C_{oi}}} + \sum_{\substack{j=1 \\ j \neq o}}^N \frac{z_j \cdot e^{C_{jo}}}{e^{C_{jk}} + \sum_{\substack{i=1 \\ i \neq j}}^N e^{C_{ji}}} \right] \\
&= -\frac{1}{N} \left[ z_{o'} \left( 1 - \frac{e^{C_{oo'}}}{e^{C_{oo'}} + \sum_{\substack{i=1 \\ i \neq o}}^N e^{C_{oi}}} \right) - \sum_{\substack{j=1 \\ j \neq o}}^N z_i \left( \frac{e^{C_{oo'}}}{e^{C_{oi}} + \sum_{\substack{i=1 \\ i \neq o}}^N e^{C_{oi}}} - \frac{e^{C_{jo}}}{e^{C_{jk}} + \sum_{\substack{i=1 \\ i \neq j}}^N e^{C_{ji}}} \right) \right] \\
&= -\frac{1}{N} \left[ z_{o'} (1 - p_+(o_{\downarrow}, o')) - \sum_{\substack{j=1 \\ j \neq o}}^N z_j (p_+(o_{\downarrow}, j) - p_+(o, j_{\downarrow})) \right]
\end{aligned} \tag{26}$$

$p_+(o_{\downarrow}, j)$  is the probability of  $z_o$  and  $z_j$  being a positive pair with  $z_o$  as the anchor sample. Similarly,  $p_+(o, j_{\downarrow})$  is the probability of  $z_o$  and  $z_j$  being a positive pair with  $z_j$  as the anchor sample. Thus, the weight of the samples with which  $z_o$  forms negative pair is the difference of the two probabilities  $p_+(o_{\downarrow}, j)$  and  $p_+(o, j_{\downarrow})$ , unlike the prediction error as in Eq. (23) when using MIO-loss.

Assuming,  $p_+$  returns hard decision probabilities, if  $(x_o, x_i)$  are false negative pairs, then  $p_+(o, i)$  in Eq. (23) and  $p_+(o_{\downarrow}, i)$  and  $p_+(o, i_{\downarrow})$  in Eq. (26) are equal to 1.0. In that case, the values of the gradients given by Eq. (23) and Eq. (26) reduces to  $\frac{1}{T_P(T_P-2)} \sum_{\substack{i=1 \\ i \neq o, o'}}^{T_P} z_i$  and 0, respectively. Hence, following gradient descent update, the direction

of movement of the feature vector  $z_o$  will be in a direction approximately opposite to the centroid of the respective class. Intuitively speaking, this phenomenon opposes collapse of representations that is often seen in contemporary self-supervised contrastive algorithms.

However, only soft probabilities are obtained using sigmoid or softmax activation functions and the negative pairings are a mixture of false and true negatives. Assuming uniform sampling of data points from each class, we can assume false negatives to consist of  $\frac{1}{|C|}$  fraction of the batch size ( $\mathcal{B}$ ) in each iteration, where  $|C|$  is the number of classes in the dataset. We can prove that the probability of obtaining approximately uniformly spaced false negative samples in the feature space is  $\left(\frac{\mathcal{B}}{|C|\mathcal{N}_{C_i}}\right)^{\frac{\mathcal{B}}{|C|}}$ , where  $\mathcal{N}_{C_i}$  is the number of samples in the class  $C_i$ . Hence, with the decrease in the number of samples per class, the resultant vector of the false negative samples becomes more similar to the centroid of their class. Thus, the gradient  $\frac{\partial \mathcal{L}_O}{\partial z_o}$  becomes diverging. If the number of classes increases, the same effect is observed. The effect of false negatives on the downstream task performance is shown in Sec. 4.2. The detailed derivations are shown in the Sec. 2.5.

## 2.5 Probability of selecting approximately symmetrically distributed false negative samples

In this section, we calculate the probability of selecting approximately symmetrically distributed false negative samples as described in the paper such that the resultant of the false negative samples is almost in the direction of the centroid of the class. First, we will calculate the probability of the selecting approximately symmetrically distributed false negative samples such that the resultant of these samples is more similar to the centroid vector than the resultant of a random combination of false negative samples. Then we will show that the magnitude of similarity of the resultant of the false negatives with the hypothetical centroid vector is always positive.

Here, we should mention that for after normalizing the samples  $z_i \in \mathbb{R}^{128}$ , the samples  $z_i$  are located on the surface of a hyper-sphere  $\mathbb{S}^{127}$ . Also for the sake of argument, we are assuming the samples are arranged symmetrically around the centroid of the respective classes on the surface of the hyper-sphere  $\mathbb{S}^{127}$ . Or in other words, we are assuming that the samples in a class are distributed according to a symmetrical multivariate normal distribution  $\mathcal{N}(M, \Sigma)$  and the centroid corresponds to the mean of the distribution. We consider that the hyper-volume which fully encircles all the samples of a particular class  $C_i$  be denoted by  $\mathbb{V}_{127}^i$ . We also denote the number of samples per class  $C_i$  by  $\mathcal{N}_{C_i}$  and the batch size by  $\mathcal{B}$ . Hence, if the samples are uniformly sampled from the dataset, then from each class  $C_i$ , we select  $\frac{\mathcal{B}}{|C|}$  samples from each class, where  $|C|$  denotes the total number of classes in the dataset. We divide  $\mathbb{V}_{127}^i$  into  $\frac{\mathcal{B}}{|C|}$  equal parts/volumes. This discretizes the enclosing volume  $\mathbb{V}_{127}^i$  into  $\frac{\mathcal{B}}{|C|}$  divisions.

Intuitively speaking, for the resultant of the false negatives to be exactly same as the centroid vector, the false negatives must be selected from each of the  $\frac{\mathcal{B}}{|C|}$  parts and each false negative sample must be equidistant from the centroid. However, when randomly selecting the false negative samples, it is not guaranteed that the the selected samples will be equidistant from the centroid. Thus, the resultant of the false negative samples cannot be same as the centroid vector. Instead, it will have some degree of similarity with it. However, a fair amount of similarity will be guaranteed if the false negative samples maintain spatial uniformity in the feature space surrounding the centroid within  $\mathbb{V}_{127}^i$ . To weakly satisfy the condition of spatial uniformity, we consider that a false negative sampled from each of  $\frac{\mathcal{B}}{|C|}$  volume of  $\mathbb{V}_{127}^i$  is sufficient.

To calculate the final expression for probability, we derive it in a few steps as follows:

- As we have already assumed the samples are arranged symmetrically around the centroid of the respective classes on the surface of the hyper-sphere  $\mathbb{S}^{127}$ , the number of samples in each discrete division of  $\mathbb{V}_{127}^i$  is  $\frac{\mathcal{N}_{C_i}|C|}{\mathcal{B}}$ .
- Since, the samples are uniformly selected from the dataset, the probability of a false negative sample being selected from the  $i$ -th division  $\mathbb{V}_{127}^i$  is  $\frac{1}{\mathcal{N}_{C_i}|C|} = \frac{\mathcal{B}}{\mathcal{N}_{C_i}|C|}$ .
- The probability of selecting a false negative sample simultaneously from each division  $\mathbb{V}_{127}^i$  is  $\left(\frac{\mathcal{B}}{\mathcal{N}_{C_i}|C|}\right)^{\frac{\mathcal{B}}{|C|}}$ .

Thus, the probability of selecting approximately symmetrically distributed false negative samples is  $\left(\frac{\mathcal{B}}{\mathcal{N}_{C_i}|C|}\right)^{\frac{\mathcal{B}}{|C|}}$ .

Now, let us see how much similar the resultant of the false negative samples is to the hypothetical centroid vector. Let us consider the  $\mathbb{R}^2$  space in Fig. 4 as our feature space of a particular class for this derivation and the location of the centroid vector be  $(x_o, y_o)$ .

Let, the position of the samples false negatives be given as follows:

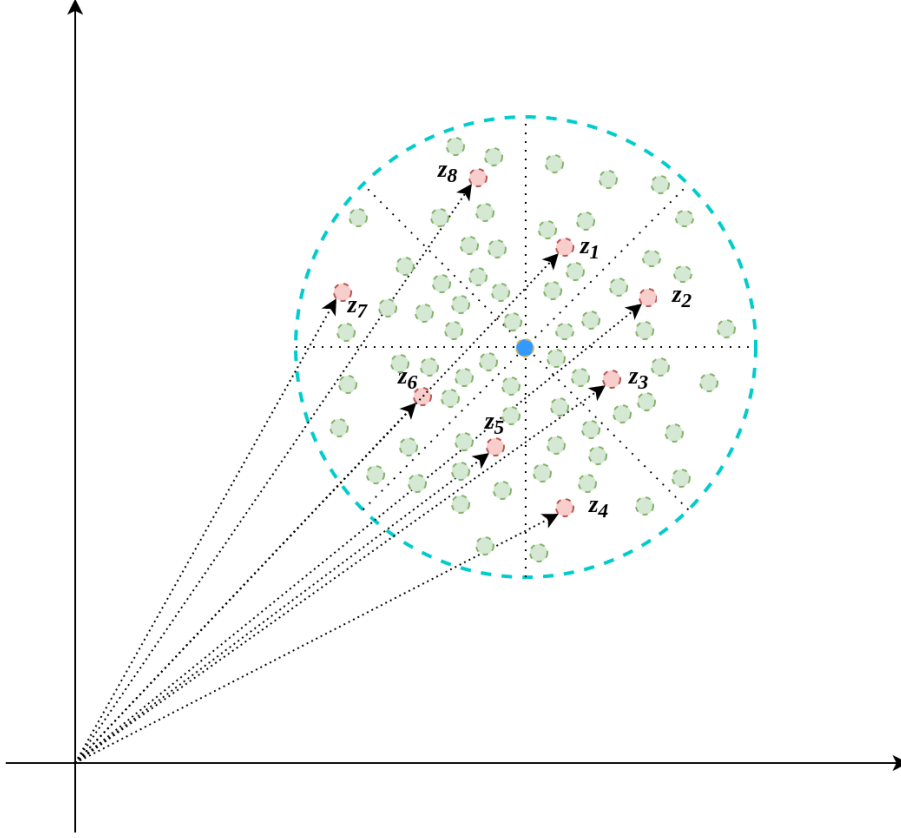


Figure 4: Illustration of arrangement of feature vectors of samples of a particular class. Red circles are the samples which have been selected. Green circles are the samples which have not been selected but are part of the class distribution. The blue circle represents the centroid of the feature cluster or the mean of the class distribution.

$$\begin{aligned} x_i &= x_o + r_i \times \cos \theta_i \\ y_i &= y_o + r_i \times \sin \theta_i \end{aligned} \quad (27)$$

where, we will assume that  $r_i$  is a random variable following the same distribution as the class distribution. Thus,  $r_i \sim \mathcal{N}(0, \sigma)$ .

From Eq. (23), the resultant of the false negatives are included in the second term inside the square brackets, which is a resultant of both false and true negatives. Here, we intend to calculate the resultant of the false negatives only. Hence, we will only consider the false negative samples. The resultant of the false negative samples is given by:

$$\begin{aligned} x' &= \frac{1}{T_P - 2} \sum_i p_i \cdot x_i = \frac{1}{T_P - 2} \sum_i p_i \cdot x_o + \frac{1}{T_P - 2} \sum_i p_i \cdot r_i \cdot \cos \theta_i = A_x + B_x \\ y' &= \frac{1}{T_P - 2} \sum_i p_i \cdot y_i = \frac{1}{T_P - 2} \sum_i p_i \cdot y_o + \frac{1}{T_P - 2} \sum_i p_i \cdot r_i \cdot \sin \theta_i = A_y + B_y \end{aligned} \quad (28)$$

From the above equations,  $A_x < x_o$  and  $A_y < y_o$  as  $0 \leq p_i \leq 1$  and  $\frac{B}{|C|} < B$ .

where,  $i = 1, 2, 3, \dots, \frac{B}{|C|}$ . We assume that  $r_i \leq 3\sigma$  of the distribution of the respective class as 99.7% of the samples lie within the region  $[\mu - 3\sigma, \mu + 3\sigma]$ . The term  $B_x$  can be expressed as:

$$\frac{1}{T_P - 2} \sum_i p_i \cdot r_i \cdot \cos \theta_i = B \cos \Theta \quad (29)$$

where,

$$0 \leq B = \sqrt{\left( \sum_i \frac{p_i \cdot r_i}{T_P - 2} \cdot \cos \theta_i \right)^2 + \left( \sum_i \frac{p_i \cdot r_i}{T_P - 2} \cdot \sin \theta_i \right)^2} \leq \sum_i \frac{p_i \cdot r_i}{T_P - 2} \leq \sum_i \frac{p_i \cdot 3\sigma}{T_P - 2} \leq \sum_i \frac{3\sigma}{T_P - 2} \leq 3\sigma$$

$$\Theta = \arctan \frac{\sum_i \frac{p_i \cdot r_i}{T_P - 2} \cdot \sin \theta_i}{\sum_i \frac{p_i \cdot r_i}{T_P - 2} \cdot \cos \theta_i} = \arctan \frac{\sum_i p_i \cdot r_i \cdot \sin \theta_i}{\sum_i p_i \cdot r_i \cdot \cos \theta_i} \quad (30)$$

Similar expressions for  $B_y$  can be obtained by replacing  $\sin \theta_i$  by  $\cos(\frac{\pi}{2} - \theta_i)$  and proceeding as Eq. (29) and Eq. (30). Hence,  $B_y = B \sin \Theta$ . From Eq. (29) and Eq. (30), we can infer that,

$$|B_x|, |B_y| < \sum_i \frac{p_i \cdot r_i}{T_P - 2} < \sum_i \frac{p_i \cdot 3\sigma}{T_P - 2} < \sum_i \frac{3\sigma}{T_P - 2} < 3\sigma \quad (31)$$

It is to be noticed that both  $x_o$  and  $y_o$  are weighted by the same factor. This plays an important role in deciding the direction of the resultant vector. The deviation from the centroid that occurs due to  $B_x$  and  $B_y$  is bounded by  $[-3\sigma, 3\sigma]$ .

Finally, the deviation from the direction of the centroid is given by :

$$\begin{aligned} \Phi &= \arctan \frac{y'}{x'} - \arctan \frac{y_o}{x_o} \\ &= \arctan \frac{\frac{1}{T_P - 2} \sum_i p_i \cdot y_o + B \sin \Theta}{\frac{1}{T_P - 2} \sum_i p_i \cdot x_o + B \cos \Theta} - \arctan \frac{y_o}{x_o} \\ &= \arctan \frac{\frac{\frac{1}{T_P - 2} \sum_i p_i \cdot y_o + B \sin \Theta}{\frac{1}{T_P - 2} \sum_i p_i \cdot x_o + B \cos \Theta} - \frac{y_o}{x_o}}{1 - \frac{\frac{1}{T_P - 2} \sum_i p_i \cdot y_o + B \sin \Theta}{\frac{1}{T_P - 2} \sum_i p_i \cdot x_o + B \cos \Theta} \frac{y_o}{x_o}} \\ &= \arctan \frac{x_o \cdot B \sin \Theta - y_o \cdot B \cos \Theta}{\frac{1}{T_P - 2} \sum_i p_i \cdot (x_o^2 - y_o^2) + x_o \cdot B \cos \Theta - y_o \cdot B \sin \Theta} \\ &= \arctan \frac{1 - \frac{y_o}{x_o} \cdot \cot \Theta}{\frac{1}{T_P - 2} \sum_i p_i \cdot \frac{(x_o^2 - y_o^2)}{x_o \cdot B \sin \Theta} + \cot \Theta - \frac{y_o}{x_o}} \end{aligned} \quad (32)$$

As the number of false negatives increases, the values of  $A_x$  and  $A_y$  approaches  $x_o$  and  $y_o$ , respectively. Also, the value of  $B_x$  and  $B_y$  also depends on the spatial uniformity of the sampled false negatives and approaches zero. In both the above cases, the deviation of the resultant of the false negatives from the actual direction of the hypothetical centroid decreases. This causes an opposite effect of pushing any particular feature vector away from the centroid during gradient descent step of the optimization process, as evident from Eq. (23). This prevents collapse of representations during the optimization process.

If all the false negative samples are symmetrically arranged around the centroid, then  $\sin \Theta \neq 0, \cos \Theta = 0$ . If the samples are equidistant from the centroid then  $p_i = p \forall i$ . Then, the value of  $\Phi$  is given by,

$$\begin{aligned} \Phi &= \arctan \frac{1}{\frac{1}{T_P - 2} \sum_i p \cdot \frac{(x_o^2 - y_o^2)}{x_o \cdot B \sin \Theta} - \frac{y_o}{x_o}} \\ &= (-1)^\xi \frac{\pi}{2} - \arctan \left( \frac{p}{T_P - 2} \cdot \eta \cdot \frac{(x_o^2 - y_o^2)}{x_o \cdot B \sin \Theta} - \frac{y_o}{x_o} \right) \end{aligned} \quad (33)$$

where  $\eta$  is the number of false negatives sampled and

$$\xi = \begin{cases} 0, & \text{if } \frac{p}{T_P-2} \cdot \eta \cdot \frac{(x_o^2 - y_o^2)}{x_o \cdot B \sin \Theta} - \frac{y_o}{x_o} > 0 \\ 1, & \text{if } \frac{p}{T_P-2} \cdot \eta \cdot \frac{(x_o^2 - y_o^2)}{x_o \cdot B \sin \Theta} - \frac{y_o}{x_o} < 0 \end{cases}$$

Hence,

$$-\frac{\pi}{2} \leq \Phi \leq \frac{\pi}{2} \quad (34)$$

The resultant of the false negative samples will always have positive cosine similarity with the hypothetical centroid vector. As evident from Eq. (23), the contribution from the false negative samples in the gradient descent step of the optimization process is negative of the resultant vector. Hence, any particular vector is pushed in a direction which is effectively at an angle of more than  $\frac{\pi}{2}$  or less than  $-\frac{\pi}{2}$  with the hypothetical centroid vector.

When the false negatives samples are not symmetrically arranged, then both  $\sin \Theta \neq \cos \Theta \neq 0$ . Then the value of  $\Phi$  is given by Eq. (32).

$$\Phi = \arctan \frac{1 - \frac{y_o}{x_o} \cdot \cot \Theta}{\frac{1}{T_P-2} \sum_i p_i \cdot \frac{(x_o^2 - y_o^2)}{x_o \cdot B \sin \Theta} + \cot \Theta - \frac{y_o}{x_o}}$$

Considering  $B \sin \Theta > 0$  and neglecting the term  $\frac{1}{T_P-2} \sum_i p_i \cdot \frac{(x_o^2 - y_o^2)}{x_o \cdot B \sin \Theta}$  as  $p_i \leq 1$  and  $T_P$  is large,

$$\begin{aligned} \Phi_+ &= \arctan \frac{1 - \frac{y_o}{x_o} \cdot \cot \Theta}{\cot \Theta - \frac{y_o}{x_o}}, \quad \text{when } Q = \frac{x_o^2 - y_o^2}{x_o} > 0 \\ \Phi_- &= \arctan \frac{1 - \frac{y_o}{x_o} \cdot \cot \Theta}{\cot \Theta - \frac{y_o}{x_o}}, \quad \text{when } Q = \frac{x_o^2 - y_o^2}{x_o} < 0 \end{aligned} \quad (35)$$

The different values of  $Q$  are shown in Fig. 5.

Hence,

$$\begin{aligned} \Phi_- &\leq \Phi \leq \Phi_+ \\ \Phi_- &\neq \Phi_+ \end{aligned} \quad (36)$$

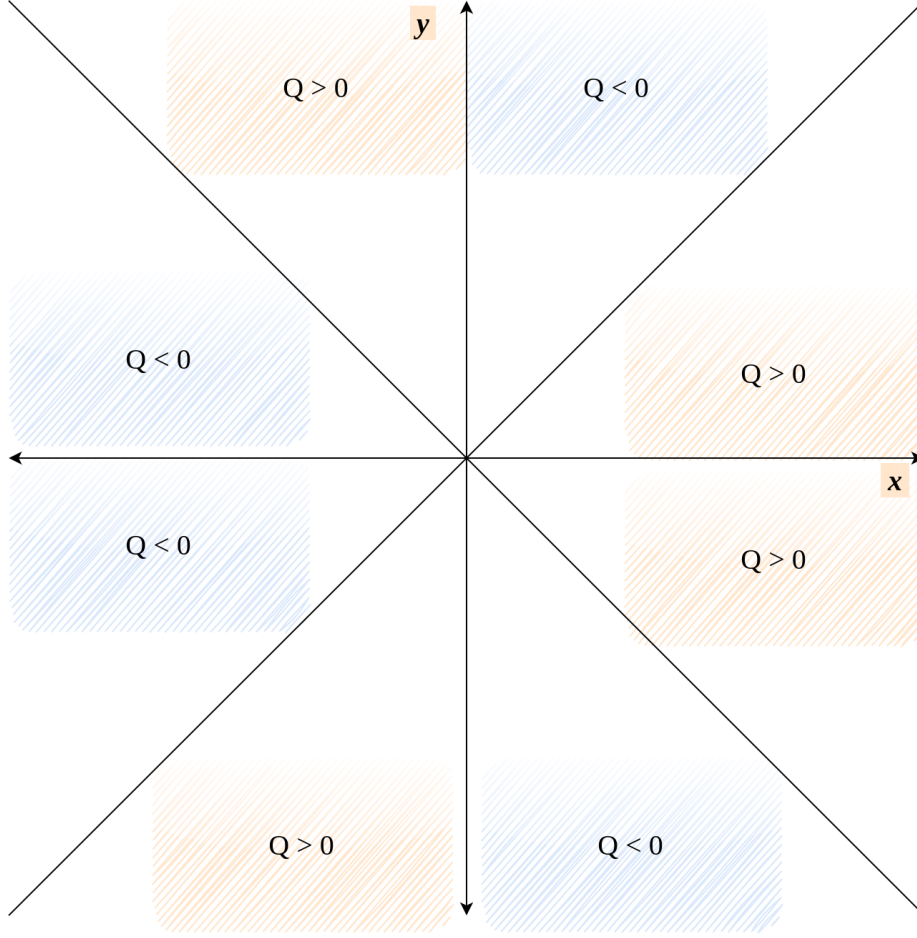
We can express  $\Phi_-$  or  $\Phi_+$  as,

$$\begin{aligned} \Phi_* &= \arctan \frac{1 - \frac{y_o}{x_o} \cdot \cot \Theta}{\cot \Theta - \frac{y_o}{x_o}} \\ \Phi_* &= (-1)^\xi \frac{\pi}{2} - \arctan \frac{\cot \Theta - \frac{y_o}{x_o}}{1 - \frac{y_o}{x_o} \cdot \cot \Theta} \\ \Phi_* &= (-1)^\xi \frac{\pi}{2} - \left[ \arctan \cot \Theta - \arctan \frac{y_o}{x_o} \right] \\ \Phi_* &= (-1)^\xi \frac{\pi}{2} - \left( \frac{\pi}{2} - \Theta \right) + \arctan \frac{y_o}{x_o} \end{aligned} \quad (37)$$

where

$$\xi = \begin{cases} 0, & \text{if } \Theta < \frac{\pi}{2} - \arctan \frac{y_o}{x_o} \\ 1, & \text{if } \Theta > \frac{\pi}{2} - \arctan \frac{y_o}{x_o} \end{cases}$$



Figure 5: Figure showing the values of  $Q$  in different quadrants.

Thus,

$$\Phi_* = \Theta + \arctan \frac{y_o}{x_o}, \text{ or } -\pi + \Theta + \arctan \frac{y_o}{x_o} \quad (38)$$

Hence, we can deduce a 4 cases for the value of the deviation  $\Phi$ , in the following table,

	$\Theta < \frac{\pi}{2} - \arctan \frac{y_o}{x_o}$	$\Theta > \frac{\pi}{2} - \arctan \frac{y_o}{x_o}$
$Q < 0$	$\Theta + \arctan \frac{y_o}{x_o}$	$-\pi + \Theta + \arctan \frac{y_o}{x_o}$
$Q > 0$	$\Theta + \arctan \frac{y_o}{x_o}$	$-\pi + \Theta + \arctan \frac{y_o}{x_o}$

Table 1: Caption

In a similar way, we can derive the values for  $\Phi$  considering  $B \sin \Theta < 0$ . From the Table 1, we can infer that  $-\frac{\pi}{2} \leq \Phi \leq \frac{\pi}{2}$ . Thus, the resultant of the false negative samples always bears positive cosine similarity with the hypothetical centroid vector or the mean of the multivariate normal class distribution.

To conclude this section, we can infer that as the number of false negatives increases, the deviation angle  $\Phi$  decreases and vice-versa. Thus, for datasets which has low number of classes, the number of false negatives per batch increases and the deviation decreases. Hence, during gradient descent step of the optimization procedure, the negative of the weighted resultant of the false negatives has a direction which is almost the opposite to the hypothetical centroid.

However, the probability of sampling symmetrically distributed samples decreases with the increase in the number of samples per class. This decreases the similarity of the resultant of the false negative samples with the hypothetical centroid. Or in other words, the deviation angle  $\Phi$  increases.

## 2.6 Adding $L_2$ Regularizer

As shown in the previous section, the change in the position of a feature vector  $z_o$  is a weighted vector sum of the feature vectors with which  $z_o$  interacts. In Eq. (23) and Eq. (26), we see that the gradient  $\frac{\partial \mathcal{L}_O}{\partial z_o}$  indicates that the feature vector  $z_o$  moves in a direction which is the resultant of two other vectors. One of those two vectors points to a direction opposite to the resultant of the feature vectors with which  $z_o$  forms a negative pair. The other is in the direction same as  $z_{o'}$ . However, this does not necessarily indicate that the two feature vectors  $z_o$  and  $z_{o'}$  of the positive pair  $(x_o, x_{o'})$  are moving towards each other in the feature space, as the optimal direction of change of position for the feature vector  $z_o$  would be  $-(z_o - z_{o'})$ . Incorporating the negative sign that will be added at the time of gradient update, the optimal direction of change can be stated as  $z_o - z_{o'}$ . To prevent the diverging of the feature vectors due to the presence of false negatives in the negative pairs, we introduce a regularizer in the form of  $L_2$  loss  $\|z_i - z_j\|_2^2$ . As the model trains more and learns better representation, the feature vectors of the samples in the positive pair would be mapped closer to each other and the value of this regularizer will automatically decrease, decreasing its contribution to the loss. Adding this regularizer to the proposed loss function, we obtain the loss function in the following form:

$$\mathcal{L}_{O+L_2} = \mathcal{L}_O + \lambda \sum_{(x_i, x_j) \sim p_+} \|z_i - z_j\|_2^2 \quad (39)$$

The value of the co-efficient  $\lambda$  is chosen such that the  $L_2$  loss does not affect  $\mathcal{L}_O$ .

## 3 Experiments and Results

In this section, at first, we are going to present the datasets that we used for our experiments and then the experimental configuration of the models we used. We also present the accuracy of the proposed model on the selected datasets and the comparison results with the state-of-the-art algorithms.

### 3.1 Datasets

We used three datasets to conduct the experiments with the proposed loss function, namely, CIFAR-10, STL-10 and CIFAR-100. The dimensions of images in CIFAR-10, STL-10, CIFAR-100 are  $32 \times 32$ ,  $96 \times 96$  and  $32 \times 32$ , respectively. The details of the distribution of the training and test set are given in Table 2.

Dataset	No. of classes	Images	
		Training	Test
CIFAR-10	10	50000	10000
STL-10	10	5000	8000
CIFAR-100	100	50000	10000

Table 2: Training and Test images distribution in different datasets

### 3.2 Pretext Experiments

In the self-supervised pre-training phase, ResNet-50 [30] has been used as the base encoder in all the experiments. However, for pre-training on CIFAR-10 and CIFAR-100 [25] datasets, the base encoder was modified according to the details provided in Appendix B.9 in [17]. But for STL-10 [24], no changes were made to the ResNet-50 [30] encoder.

For the proposed model, the projector contains 2 hidden layers of 2048 units having 1D Batch Normalization [31] and ReLU [32] activation after each hidden layer, followed by the output layer having 128 units. However, in the ablation studies, we have used a projector with 1 hidden layer also.

For pre-training the proposed model, we used a batch size of 128 on a single 16GB NVIDIA V100 GPU on Google Colab. As the batch size was 128, we can obtain  $128 \times 2 = 256$  augmented samples forming 256 positive pairs and  $4 \times 128^2 - 4 \times 128 = 65024$  negative pairs.

We used LARS [33] optimizer along with a cosine decay schedule with a linear warmup schedule for 10 epochs. The maximum epoch number was set to 1000 to ensure a slow learning rate decay. The learning rate used in the pre-training phase is 1.5 and the temperature parameter is chosen to be 0.5. The detailed ablations for the learning rate and temperature parameter are given in Sec. 4.1. We pre-trained the model for 250 epochs following the configuration mentioned above. When using the  $L_2$  regularizer as described in Sec. 2.6, the value of hyper-parameter lambda was chosen according to the constraint described in Sec. 2.6.

For reproducing the state-of-the-art algorithms on self-supervised representation learning, we applied the configuration used in the official implementations. Thus, our work also provides a benchmark on the performance of the state-of-the-art models on datasets like STL-10 [24], CIFAR-10 and CIFAR-100 [25].

### 3.2.1 Augmentation Details

The augmentations used for training the models using MIO-loss are included below in Table 3. For this section, let the input dimension be denoted by  $l$  and the scale factor be denoted by  $s$ . Also,  $p$  denotes the probability of randomly applying a particular augmentation.

Augmentations	Details
Random Horizontal Flipping	$p = 0.5$
Random Resized Cropping	Output dimension = $l$ $p = 0.5$
Random Color Jitter	Brightness $\in [-0.8s, 0.8s]$
	Contrast $\in [-0.8s, 0.8s]$
	Saturation $\in [-0.8s, 0.8s]$
	Hue $\in [-0.2s, 0.2s]$
Random Grayscale	$p = 0.2$
Random Gaussian Blur	Applied only if $l > 32$
	kernel size = $\text{int}(\frac{l}{10})$ if $l$ is even, else $\text{int}(\frac{l}{10}) + 1$ $\sigma \in [0.1, 2.0]$
Random Solarize	threshold = 0.5
	$p = 0.2$

Table 3: Augmentations used for obtaining a transformed positive pair of samples from an input image.

### 3.3 Downstream Experiments

For the downstream experiments, we conducted a linear evaluation on the respective datasets. In self-supervised representation learning, the quality of the representations learned by the model is evaluated by the performance of the pre-trained model on linear classification task. As the dimensions of the samples in the datasets are not greater than  $96 \times 96$ , we chose image classification task for linear evaluation.

For the linear classification phase, we intend to evaluate all the models with the same training configurations. We trained the linear classifier using an SGD optimizer with an initial learning rate of 0.01 and an exponential decay of 0.98 per epoch for 100 epochs with early stopping. The batch size used in the linear classification experiments is 32. Training all models with the same experimental configurations allows a fair comparison of the representations learned by the different models. The comparison results obtained with different state-of-the-art algorithms on different datasets are presented in Sec. 3.4.

### 3.4 Results

In this subsection, we present the comparative results of linear classification of the state-of-the-art self-supervised algorithms, namely, SimCLR [17], MoCoV2 [19], BYOL [20], SimSiam [21] and Barlow Twins [22] on STL-10, CIFAR-10 and CIFAR-100 datasets. We present the results of four models, named (A), (B), (C) and (D). Model (A) and (B) were trained with a projector containing 1 and 2 hidden layers, respectively, without  $L_2$  regularizer. Model (C) and (D) represents the same models as (A) and (B), respectively, but with added  $L_2$  regularizer having  $\lambda = 1.0$ . The best and second best performing algorithms are marked in bold and colored in blue, respectively. In the column named "Best", we present the best results for the proposed algorithm on CIFAR-10 (Model (D)), CIFAR-100 (Model (D)) and STL-10 (Model (D), Batch Size = 32) datasets.

Dataset	SimCLR	MoCov2	BYOL	SimSiam	Barlow Twins	Ours(MIO)				
						(A)	(B)	(C)	(D)	Best
CIFAR-10	85.24	81.68	83.33	76.03	75.21	84.31	84.55	<b>85.40</b>	<b>85.44</b>	<b>85.44</b>
CIFAR-100	56.23	51.90	55.86	29.45	51.14	55.33	<b>56.71</b>	55.78	<b>56.81</b>	<b>56.81</b>
STL-10	52.50	41.70	52.14	52.18	55.29	58.1	<b>59.61</b>	58.73	<b>60.25</b>	<b>60.75</b>

Table 4: Comparative results of the state-of-the-art self-supervised algorithms on CIFAR-10, CIFAR-100 and STL-10 datasets.

From the Table 4, it is evident that our best model outperforms the state-of-the-art algorithms on all the three datasets CIFAR-10, CIFAR-100 and STL-10. Thus, with the constraints of low dimensional input images, a low number of training samples and limited training epochs, we can clearly state that the proposed model stands out above the other models used in the comparison.

## 4 Ablation Studies

In this section, we present the results of the ablation study on hyper-parameters  $\lambda$  and batch size. This ablation study aims to observe the change in performance of the proposed model on the STL-10 and CIFAR-10 datasets.

### 4.1 Ablations on Learning Rate and Temperature

For choosing the optimal temperature hyper-parameter, we conducted experiments with a learning rate of 0.3 for temperature values of 0.3, 0.5 and 0.7 and obtained test accuracy of 74.9%, 76.98% and 74.219%, respectively. Hence, the optimal value of temperature was chosen as 0.5.

For choosing the optimal learning rate for our experiments, we conducted ablations studies on CIFAR-10 [25]. The linear classification performance of Model (A) (as given in Table 4) pre-trained with temperature value of 0.5 for 100 epochs on CIFAR-10 with learning rates 0.3, 0.5, 1.0, 1.5 and 2.0 are 76.98%, 78.61%, 80.35%, 81.25% and 80.06%, respectively. As the best performance is obtained for learning rate 1.5, we use this value for all our experiments.

### 4.2 Ablation on Batch Size

Contrastive learning algorithms like SimCLR [17], MoCoV2 [19], BYOL [20] usually requires a large number of samples in a single batch to learn good representations. The performance of these SOTA algorithms depends on the batch size used in the pre-training phase. In this subsection, we are going to explore the effects of varying the batch size in the pre-training phase on the performance of the proposed model on STL-10 [24] and CIFAR-10 [25] datasets. From the Fig. 6, we can see that for the STL-10 dataset, the performance improves when batch size is decreased. In contrast, an opposite phenomenon is observed for CIFAR-10. The STL-10 dataset contains 500 images per class and this makes the dataset relatively sparse compared to CIFAR-10. Taking into consideration the explanation provided in Sec. 2.4.1, we can understand the reason behind the observed contrasting behavior in STL-10 and CIFAR-10 datasets.

### 4.3 Ablation on hyper-parameter $\lambda$

In this subsection, we perform ablation on the hyper-parameter  $\lambda$ , co-efficient of the  $L_2$  regularizer (Sec. 2.6) added to the base loss  $\mathcal{L}_O$ . The drop in performance at high values of  $\lambda$  for STL-10 [24] dataset may be attributed to the fact that as the  $\lambda$  value grows, the  $L_2$  regularizer part becomes more contributing in the loss  $\mathcal{L}_{O+L_2}$  and it approaches the loss function used in BYOL [20]. However, as we are not using a predictor like in [20], this leads to a collapse of representations.

Similar behavior can be observed for CIFAR-10 [25] dataset also. However, the optimal value of  $\lambda$  is not same for the datasets. We can see the variation of test accuracy over different values of  $\lambda$  in the Fig. 7.

### 4.4 Ablation on number of hidden layer in Projector

From [17], we know that using a non-linear projector improves the quality of representations from the encoder. Using a non-linear projector, we see an improvement in performance in [19] over [18]. Similarly, all the methods [20, 21, 22] use non-linear projectors with 2 or more layers. We use projectors with 1 and 2 hidden layers for this ablation study. Fig. 8 shows the performance of the different models on STL-10 [24] and CIFAR-10 [25] datasets.

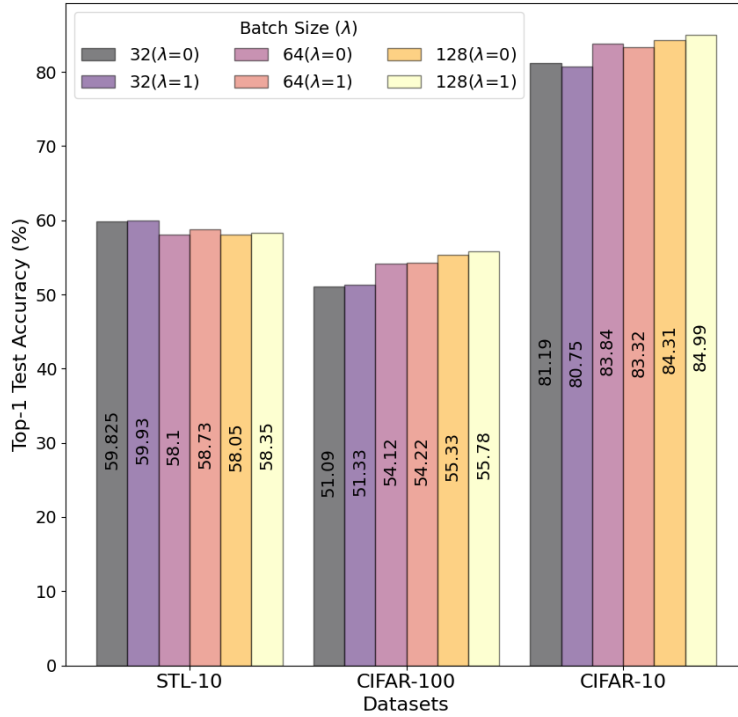


Figure 6: Ablation study of performance of the proposed model on STL-10, CIFAR-100 and CIFAR-10 datasets for different batch sizes. The projector of the model used in pre-training consisted of 1 hidden layer with 2048 units.

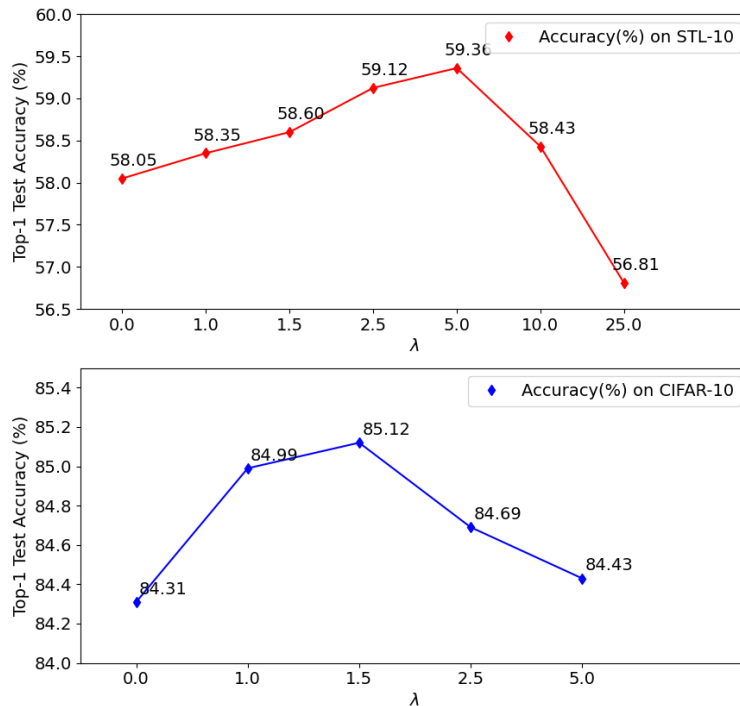


Figure 7: Ablation study on the effect of variation of hyper-parameter  $\lambda$  on the test accuracy in linear classification task achieved by the proposed model pretrained with batch size 128 on STL-10 and CIFAR-10 datasets. The projector of the model used in pre-training consisted of 1 hidden layer with 2048 units.

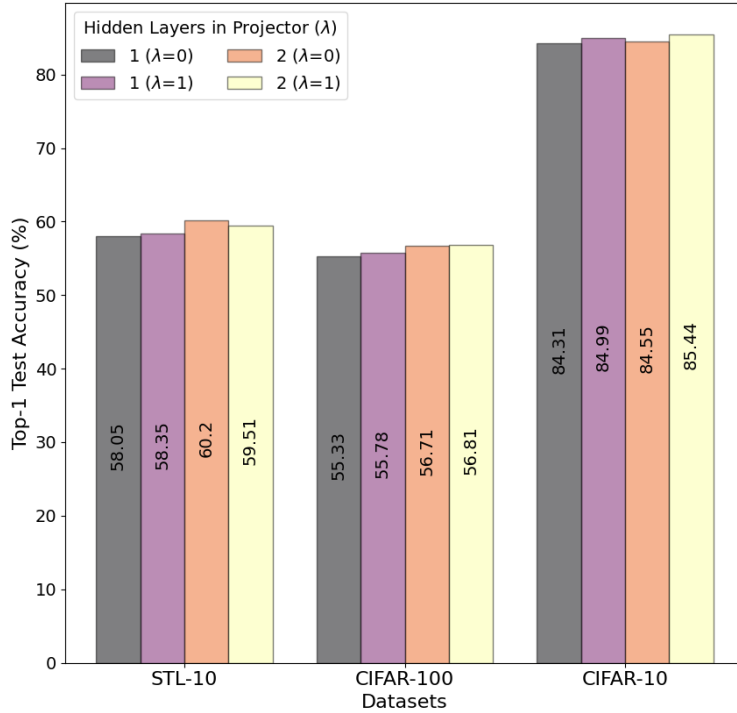


Figure 8: Ablation study of the effect of number of hidden layers in the projector on the performance of the proposed model on STL-10, CIFAR-100 and CIFAR-10 datasets. All the experiments for this ablation study were conducted with batch size 128.

#### 4.5 Ablation on Encoder Architecture

In this section, we present the ablation study on the number of parameters of the encoder or encoder architectures on the performance on STL-10 dataset. For this ablation study, we conducted experiments with ResNet-34, ResNet-50, ResNet-101, ResNet-152. The projector used in the experiments used only 1 hidden layer and the output dimension was 128. Also, the batch size used in the experiments was 32. Experiments were conducted for  $\lambda = 0.0, 1.0$ . The performance of the models are presented in Fig. 9. The performance results shows that the architecture ResNet-50 performs the best among all the architectures.

## 5 Conclusion

In this work, we proposed a novel contrastive loss function, MIO-loss, that optimizes the mutual information between samples in positive and negative pairs. We also used  $L_2$  loss as a regularizer with the MIO-loss function to further improve our proposed model’s performance. Through mathematical calculation, we provide a lower bound of the proposed loss function, which is the difference between the mutual information of the samples in the negative and positive pairs. The expressions for the parameter gradients flowing into the projector and the gradient of change in position of the feature vectors provide an insight into the working principle of contrastive learning. Furthermore, through various ablation studies, we also show the variation of performance of the proposed model with the variation of different hyper-parameters. Finally, we observe that the proposed model outperforms the SOTA algorithms.

## References

- [1] L. Jing and Y. Tian, “Self-supervised spatiotemporal feature learning by video geometric transformations,” *ArXiv*, vol. abs/1811.11387, 2018. 2
- [2] S. Gidaris, P. Singh, and N. Komodakis, “Unsupervised representation learning by predicting image rotations,” in *6th International Conference on Learning Representations, ICLR 2018, Vancouver, BC, Canada, April 30 - May 3, 2018, Conference Track Proceedings*, OpenReview.net, 2018. 2

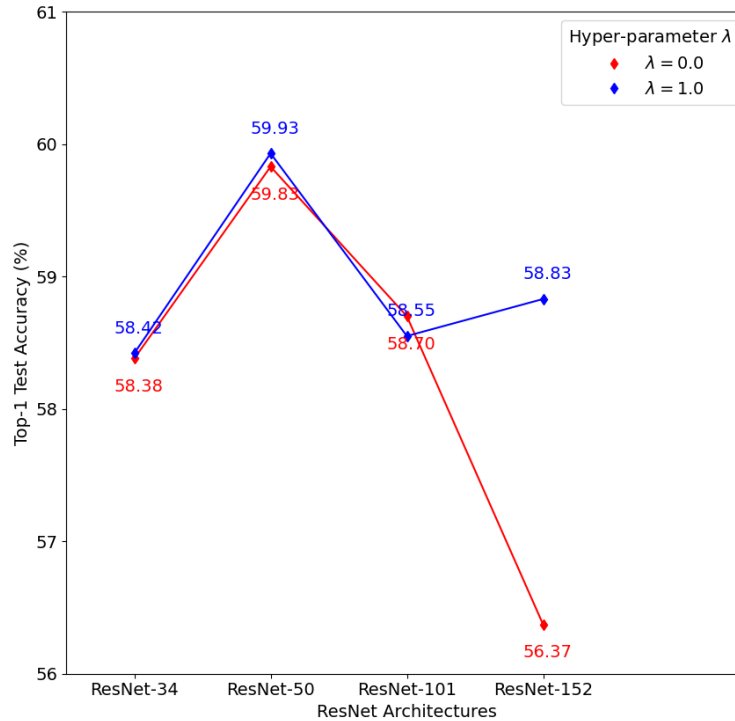


Figure 9: Ablation study on the effect of number of parameters on the test accuracy of the proposed model on STL-10 dataset.

- [3] L. Jing, X. Yang, J. Liu, and Y. Tian, “Self-supervised spatiotemporal feature learning via video rotation prediction,” *arXiv: Computer Vision and Pattern Recognition*, 2018. 2
- [4] C. Doersch, A. Gupta, and A. A. Efros, “Unsupervised visual representation learning by context prediction,” *2015 IEEE International Conference on Computer Vision (ICCV)*, pp. 1422–1430, 2015. 2
- [5] D. Pathak, P. Krähenbühl, J. Donahue, T. Darrell, and A. A. Efros, “Context encoders: Feature learning by inpainting,” *2016 IEEE Conference on Computer Vision and Pattern Recognition (CVPR)*, pp. 2536–2544, 2016. 2
- [6] M. Noroozi and P. Favaro, “Unsupervised learning of visual representations by solving jigsaw puzzles,” in *Computer Vision – ECCV 2016* (B. Leibe, J. Matas, N. Sebe, and M. Welling, eds.), (Cham), pp. 69–84, Springer International Publishing, 2016. 2
- [7] U. Ahsan, R. Madhok, and I. Essa, “Video jigsaw: Unsupervised learning of spatiotemporal context for video action recognition,” *2019 IEEE Winter Conference on Applications of Computer Vision (WACV)*, pp. 179–189, 2019. 2
- [8] C. Wei, L. Xie, X. Ren, Y. Xia, C. Su, J. Liu, Q. Tian, and A. Yuille, “Iterative reorganization with weak spatial constraints: Solving arbitrary jigsaw puzzles for unsupervised representation learning,” *2019 IEEE/CVF Conference on Computer Vision and Pattern Recognition (CVPR)*, pp. 1910–1919, 2019. 2
- [9] D. Kim, D. Cho, D. Yoo, and I.-S. Kweon, “Learning image representations by completing damaged jigsaw puzzles,” *2018 IEEE Winter Conference on Applications of Computer Vision (WACV)*, pp. 793–802, 2018. 2
- [10] F. Siar, A. Gheibi, and A. Mohades, “Unsupervised learning of visual representations by solving shuffled long video-frames temporal order prediction,” *ACM SIGGRAPH 2020 Posters*, 2020. 2
- [11] H. Buckchash and B. Raman, “Sustained self-supervised pretraining for temporal order verification,” in *Pattern Recognition and Machine Intelligence - 8th International Conference, PReMI 2019, Tezpur, India, December 17-20, 2019, Proceedings, Part I* (B. Deka, P. Maji, S. Mitra, D. K. Bhattacharyya, P. K. Bora, and S. K. Pal, eds.), vol. 11941 of *Lecture Notes in Computer Science*, pp. 140–149, Springer, 2019. 2
- [12] D. Xu, J. Xiao, Z. Zhao, J. Shao, D. Xie, and Y. Zhuang, “Self-supervised spatiotemporal learning via video clip order prediction,” *2019 IEEE/CVF Conference on Computer Vision and Pattern Recognition (CVPR)*, pp. 10326–10335, 2019. 2
- [13] A. El-Nouby, S. Zhai, G. W. Taylor, and J. Susskind, “Skip-clip: Self-supervised spatiotemporal representation learning by future clip order ranking,” *ArXiv*, vol. abs/1910.12770, 2019. 2
- [14] I. Misra, C. L. Zitnick, and M. Hebert, “Shuffle and learn: Unsupervised learning using temporal order verification,” in *ECCV*, 2016. 2

- [15] J. Wang, J. Jiao, and Y.-H. Liu, “Self-supervised video representation learning by pace prediction,” in *Computer Vision – ECCV 2020* (A. Vedaldi, H. Bischof, T. Brox, and J.-M. Frahm, eds.), (Cham), pp. 504–521, Springer International Publishing, 2020. [2](#)
- [16] R. Zhang, P. Isola, and A. A. Efros, “Colorful image colorization,” in *Computer Vision – ECCV 2016* (B. Leibe, J. Matas, N. Sebe, and M. Welling, eds.), (Cham), pp. 649–666, Springer International Publishing, 2016. [2](#)
- [17] T. Chen, S. Kornblith, M. Norouzi, and G. E. Hinton, “A simple framework for contrastive learning of visual representations,” in *Proceedings of the 37th International Conference on Machine Learning, ICML 2020, 13-18 July 2020, Virtual Event*, vol. 119 of *Proceedings of Machine Learning Research*, pp. 1597–1607, PMLR, 2020. [2](#), [3](#), [18](#), [19](#), [20](#)
- [18] K. He, H. Fan, Y. Wu, S. Xie, and R. B. Girshick, “Momentum contrast for unsupervised visual representation learning,” in *2020 IEEE/CVF Conference on Computer Vision and Pattern Recognition, CVPR 2020, Seattle, WA, USA, June 13-19, 2020*, pp. 9726–9735, IEEE, 2020. [2](#), [20](#)
- [19] X. Chen, H. Fan, R. B. Girshick, and K. He, “Improved baselines with momentum contrastive learning,” *CoRR*, vol. abs/2003.04297, 2020. [2](#), [19](#), [20](#)
- [20] J.-B. Grill, F. Strub, F. Altché, C. Tallec, P. Richemond, E. Buchatskaya, C. Doersch, B. Avila Pires, Z. Guo, M. Gheshlaghi Azar, B. Piot, k. kavukcuoglu, R. Munos, and M. Valko, “Bootstrap your own latent - a new approach to self-supervised learning,” in *Advances in Neural Information Processing Systems* (H. Larochelle, M. Ranzato, R. Hadsell, M. F. Balcan, and H. Lin, eds.), vol. 33, pp. 21271–21284, Curran Associates, Inc., 2020. [2](#), [19](#), [20](#)
- [21] X. Chen and K. He, “Exploring simple siamese representation learning,” in *Proceedings of the IEEE/CVF Conference on Computer Vision and Pattern Recognition (CVPR)*, pp. 15750–15758, June 2021. [2](#), [19](#), [20](#)
- [22] J. Zbontar, L. Jing, I. Misra, Y. LeCun, and S. Deny, “Barlow twins: Self-supervised learning via redundancy reduction,” in *ICML*, 2021. [2](#), [19](#), [20](#)
- [23] A. van den Oord, Y. Li, and O. Vinyals, “Representation learning with contrastive predictive coding,” *ArXiv*, vol. abs/1807.03748, 2018. [2](#), [3](#), [9](#), [10](#)
- [24] A. Coates, A. Ng, and H. Lee, “An analysis of single-layer networks in unsupervised feature learning,” in *Proceedings of the Fourteenth International Conference on Artificial Intelligence and Statistics* (G. Gordon, D. Dunson, and M. Dudík, eds.), vol. 15 of *Proceedings of Machine Learning Research*, (Fort Lauderdale, FL, USA), pp. 215–223, PMLR, 11–13 Apr 2011. [2](#), [18](#), [19](#), [20](#)
- [25] A. Krizhevsky, “Learning multiple layers of features from tiny images,” pp. 32–33, 2009. [2](#), [18](#), [19](#), [20](#)
- [26] C. E. Shannon, “A mathematical theory of communication,” *The Bell System Technical Journal*, vol. 27, no. 3, pp. 379–423, 1948. [5](#)
- [27] T. M. Cover and J. A. Thomas, *Elements of Information Theory (Wiley Series in Telecommunications and Signal Processing)*. USA: Wiley-Interscience, 2006. [5](#)
- [28] D. McAllester and K. Stratos, “Formal limitations on the measurement of mutual information,” in *Proceedings of the Twenty Third International Conference on Artificial Intelligence and Statistics* (S. Chiappa and R. Calandra, eds.), vol. 108 of *Proceedings of Machine Learning Research*, pp. 875–884, PMLR, 26–28 Aug 2020. [5](#)
- [29] D. Koller and N. Friedman, *Probabilistic Graphical Models: Principles and Techniques - Adaptive Computation and Machine Learning*. The MIT Press, 2009. [5](#)
- [30] K. He, X. Zhang, S. Ren, and J. Sun, “Deep residual learning for image recognition,” *2016 IEEE Conference on Computer Vision and Pattern Recognition (CVPR)*, pp. 770–778, 2016. [18](#)
- [31] S. Ioffe and C. Szegedy, “Batch normalization: Accelerating deep network training by reducing internal covariate shift,” in *Proceedings of the 32nd International Conference on Machine Learning* (F. Bach and D. Blei, eds.), vol. 37 of *Proceedings of Machine Learning Research*, (Lille, France), pp. 448–456, PMLR, 07–09 Jul 2015. [18](#)
- [32] K. He, X. Zhang, S. Ren, and J. Sun, “Delving deep into rectifiers: Surpassing human-level performance on imagenet classification,” *2015 IEEE International Conference on Computer Vision (ICCV)*, pp. 1026–1034, 2015. [18](#)
- [33] Y. You, I. Gitman, and B. Ginsburg, “Large batch training of convolutional networks,” 2017. [19](#)